

# Towards Intelligent Cross-Domain Resource Coordinate Scheduling for Satellite Networks

Chenxi Bao, Min Sheng\*, Senior Member, IEEE, Di Zhou, Member, IEEE, Yan Shi, Jiandong Li, Fellow, IEEE

**Abstract**—The new generation satellite network is a comprehensive service system that can provide communication, observation, navigation, and other functions. Typically, a system with a specific service function is defined as a domain and the supply and demand relationship of resources, such as communication, storage, and energy resources, are unbalanced among domains. Therefore, it is nontrivial to accurately characterize the cross-domain resource state and coordinate the data transmission policy of interrelated satellites from different domains to make full use of the resources in each domain aiming at improving the resource utilization ratio (RUR) of the whole network. To this end, this paper investigates the cross-domain resource scheduling (CDRS) problem in satellite networks aiming at maximizing the total amount of downloaded transmitted data. We start with the orbit motion law of satellites and construct the satellite orbit feature matrix of each domain to design a hierarchical sparse resource representation (HSRR) scheme to accurately characterize the resource state of each domain in real-time with low complexity. Further, based on the HSRR, we develop a cross-domain dynamic multi-resource scheduling algorithm to solve the CDRS problem by introducing the advantage factor and policy-oriented hyper-parameter. The algorithm can make full use of the resources in each domain to achieve efficient CDRS by dynamically adjusting the data transmission policy of satellites among domains. Simulation results show that the greater the service demand and resource difference among domains, the more significant the performance improvement brought by CDRS, and compared with the existing algorithms, the RUR and resource utilization efficiency have been significantly improved.

**Index Terms**—Satellite networks, sparse resource representation, resource scheduling, multi-agent reinforcement learning.

## I. INTRODUCTION

With the rapid development of the fifth-generation communication system, various things are widely connected [1], [2]. It is estimated that by 2025, the number of connected devices globally will skyrocket to 30 billion [3]. However, for remote areas such as seas, and mountain zones, traditional ground infrastructures are still difficult to deploy [4]. The satellite network will play an important role in realizing global ubiquitous communication [5], which is being considered by the sixth-generation communication system in the future [6]–[8]. Moreover, the combination of satellite communication and

This work was supported in part by the Natural Science Foundation of China under Grant 62121001, U19B2025, and 62001347, in part by Key Research and Development Program of Shaanxi (Program No. 2022ZDLGY05-02), in part by Young Elite Scientists Sponsorship Program by CAST (Program No. 2022QNRC001), and in part by Young Talent Support Program of Xi'an Association for Science and Technology (No. 095920221337). (Corresponding author: Min Sheng.)

Chenxi Bao, Min Sheng, Di Zhou, Yan Shi, and Jiandong Li are with the State Key Laboratory of Integrated Service Networks, Xidian University, Xi'an, Shaanxi, 710071, China. (e-mail: cxba@stu.xidian.edu.cn; {zhoudi, yshi}@xidian.edu.cn; {msheng, jdli}@mail.xidian.edu.cn).

terrestrial wireless communication has attracted the attention of many researchers and companies. For example, OneWeb, SpaceX, and other companies [9]–[11] are committed to constructing satellite networks with thousands of satellites to improve the network capacity.

The satellite network is a comprehensive service system that can provide multiple types of service functions, and a system with a specific service function is usually defined as a domain. However, since the global data service demands are growing rapidly [12] and there are obvious differences in service attributes among domains, the supply and demand of resources among domains are seriously imbalanced. For example, observation satellites are usually only responsible for observing a target or area on the ground [13]. Since the observation satellite can collect data only when the observation target or area is within the capture range of its imager, even if the amount of data collected each time is large, the demands of conventional missions are still sparse for an observation satellite. This means that the resource utilization ratio (RUR) of the whole network can be improved by using satellites with low service or non-busy service to assist satellites with high service or busy service to offload data. Therefore, in order to reasonably allocate the resources used by satellites to transmit data from different domains, the cross-domain resource scheduling (CDRS) problem should be focused on to achieve the best data transmission performance and higher RUR.

It is a technical challenge to develop an efficient CDRS scheme in satellite networks. On the one hand, resource representation is the key technology of efficient resource scheduling. However, satellite networks include satellites with multiple service attributes, which are located at different orbit altitudes, and due to the high-speed orbit motion of satellites, the satellite network topology is complex, changeable, and highly dynamic. Therefore, how to accurately characterize communication resources with low complexity is very important to achieve efficient CDRS. On the other hand, the efficient coordination of resources among domains is an important means to improve the RUR of the whole network. However, the coordinated scheduling of resources among domains needs to consider the service demands and resources of the whole network, which has higher solution complexity compared with a single domain. Therefore, how to reasonably allocate the resources of each domain and achieve efficient CDRS, so as to improve the RUR of the whole network, is a difficult problem. In fact, it is a process of constantly adjusting the resource scheduling policy and seeking the dynamic balance of resource scheduling.

To the best of our knowledge, the CDRS problem remains almost untouched. To this end, we first propose a hierarchical sparse resource representation (HSRR) scheme, which can accurately characterize the communication resources of satellite networks in real-time with low complexity. Based on the HSRR, we convert the CDRS problem to a Markov decision problem (MDP). Furthermore, we propose a cross-domain dynamic multi-resource scheduling (CD-DMRS) algorithm. Our major contributions are summarized as follows:

- We start with the orbit motion law of satellites and utilize the periodicity and rotational closure of the inter-satellite connection relationship (ISCR) to design an intra-layer sparse representation scheme. Then, we construct the satellite orbit feature matrix (SOFM) to deduce the network topology among domains to design an inter-layer sparse representation scheme. Intra-layer sparse representation and inter-layer sparse representation jointly realize the HSRR and the real-time representation of satellite communication resources, which can effectively reduce the space complexity of resource representation for satellite networks.
- Since the traditional optimization method needs to characterize the ISCRs of all time slots in advance, to solve the CDRS problem, it will bring high space complexity. However, thanks to the proposed real-time representation of communication resources, it is possible to perform global resource scheduling without obtaining all ISCRs in advance. Therefore, we model the CDRS problem as the MDP and expect to maximize the long-term reward of the whole network.
- Based on the HSRR, we apply a deep neural network (DNN) to multi-agent reinforcement learning (MARL) and develop a CD-DMRS algorithm to solve the CDRS problem by introducing the advantage factor and policy-oriented hyper-parameter. The algorithm can dynamically adjust the resource scheduling policy of interrelated satellites according to the resource states of each domain by learning the mapping relationship between the resource states and the scheduling policy.
- Extensive simulation results are provided to validate the efficacy of the proposed algorithm. Simulation results show that the greater the service demand and resource difference among domains, the more significant the performance improvement brought by CDRS. Besides, the CD-DMRS algorithm achieves higher performance in terms of RUR and resource utilization efficiency (RUE) compared with existing algorithms.

The rest of this paper is organized as follows. Section II describes the related work, followed by the system model and problem formulation in Section III. In Section IV, the HSRR scheme and the CDRS problem equivalent conversion are introduced in detail. We propose a CD-DMRS algorithm to solve the CDRS problem in Section V. Section VI provides the simulation results, finally, conclusions are drawn in Section VII.

## II. RELATED WORK

Resource scheduling problem has always been a research hotspot in satellite networks, and the research of resource scheduling is usually accompanied by resource representation. In particular, the CDRS puts forward higher requirements for resource representation. Therefore, we briefly introduce the recent research on resource representation and resource scheduling.

The snapshots sequence graph (SSG) and time-expanded graph (TEG) are important tools to characterize the dynamic change of the network topology. SSG is widely used to characterize the connections between nodes in various networks, such as social networks [14], [15], communication networks [16], [17], and satellite networks [18]. However, SSG cannot efficiently describe the relationship between snapshots and the impact of network topology changes. TEG uses storage arcs to connect discrete time snapshots to model the impact of network topology change on data transmission. In [19], [20], TEG is used to explore the routing problem of satellite networks. A storage time aggregated graph (STAG) that can effectively reduce the storage space occupied by SSG and TEG was proposed in [21]. In addition, Haiquan Sun *et al.* used the time window to describe the visible start and end times between satellites [22]. In satellite networks, SSG and TEG occupy a lot of storage space due to each snapshot containing thousands of satellites. Although STAG can effectively reduce the occupied storage, it still needs to characterize the resources of all time slots. The time window also has such a problem.

Based on the above resource representation schemes, resource scheduling problems have been widely studied and can be classified into two main categories: single service attribute and multiple service attributes. The resource scheduling schemes of satellite networks with the single service attribute were considered in [23], [24]. Di Zhou *et al.* focused on the partially known distribution information of long-term service arrival and proposed a robust two-stage stochastic optimization framework on the extended TEG [23]. An improved feedback structure heuristic algorithm for resource scheduling of earth observation satellites was proposed in [24]. Furthermore, the resource scheduling schemes of a typical three-layer data relay satellite network based on time window were focused on [25], [26]. The dynamic scheduling problem of hybrid services was focused and the resource scheduling scheme could significantly increase the time average number of hybrid services [25]. A service scheduling model considering that a single service was divided into multiple subtasks for transmission was proposed [26]. Although the existing research on satellite networks with multiple service attributes considers the satellites with various functions in the user layer, the satellites with different functions cannot communicate with each other, and the services can only realize data forwarding through relay satellites. Furthermore, the relay satellites are usually composed of satellites in higher orbits, such as geosynchronous satellites, and do not have local data. Different from it, there are no specific relay satellites in the CDRS scenario, and the satellites with different functions can communicate with each other. In this case, each satellite has both the function of a user

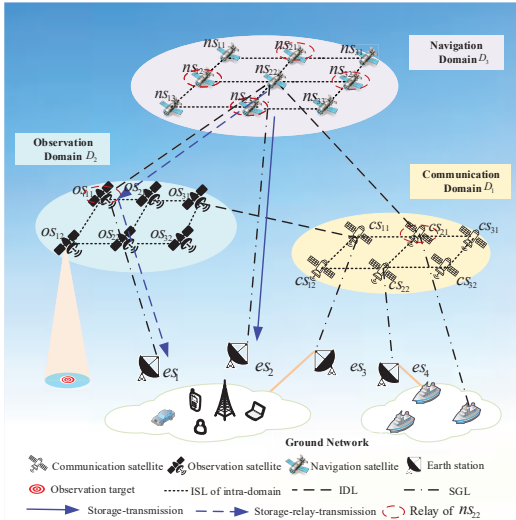


Figure 1. An example of the satellite network model.

satellite and the function of a relay satellite, and each satellite will assist others to offload data.

To sum up, the existing resource representation schemes have high space complexity, and the existing resource scheduling algorithms are mainly applied to satellite networks with a single service attribute. Moreover, in the existing research on resource scheduling for satellite networks with multiple service attributes, collaborative data offloading between satellites with different functions is not considered. Therefore, the existing resource representation and resource scheduling schemes cannot be used to solve the CDRS problem. Different from the existing work, starting from the satellite motion law, we design the HSRR scheme, which can greatly reduce the space complexity of communication resource representation, and apply MARL to the CDRS of satellite networks to obtain better adaptability to different environments.

### III. SYSTEM MODEL AND PROBLEM FORMULATION

In this section, we first describe the satellite network scenario, then introduce the channel model, the data arrival model, and the energy model. Finally, the problem formulation is elaborated. The key abbreviations and notations are shown in Table I.

#### A. Network Model

We consider a typical satellite network scenario consisting of three different service functional domains as shown in Fig. 1, i.e., the satellite communication domain, observation domain, and navigation domain, denoted by  $D_1$ ,  $D_2$ , and  $D_3$ , which includes a set of the communication satellites  $CS = \{cs_{11}, \dots, cs_{ij}, \dots, cs_{T_1, T_2}\}$ , a set of observation satellites  $OS = \{os_{11}, \dots, os_{ij}, \dots, os_{T_2, T_3}\}$ , a set of navigation satellites  $NS = \{ns_{11}, \dots, ns_{ij}, \dots, ns_{T_3, T_1}\}$ , and a set of earth stations  $ES = \{es_1, \dots, es_g, \dots, es_{N_{es}}\}$ . Further, we define  $v_{ij}(D_k)$  represents the  $j$ -th satellite in the  $i$ -th orbit in the  $k$ -th domain, where  $k \in \{1, 2, 3\}$  is the index of domains,  $i$  is the index of orbit and  $j$  is the index of the satellite. Earth

stations are used as receivers to receive data offloaded from all satellites to the ground.

In the satellite network, the three domains are auxiliary domains to each other, i.e., while completing its data offloading, satellites may also assist others to complete data transmission<sup>1</sup>. We assume that the data collected in the current time slot is transmitted in the next time slot, and the duration of time slot  $t$  is the same, which is fixed as  $\tau$ , where  $t = \{1, 2, \dots, T\}$  is the index of the time slot and  $T$  is the total number of time slots. Meanwhile, in our model, the data collected/generated in each domain arrives directly at the satellites, and the data are expected to be successfully offloaded to earth stations through two transmission modes, namely, (1) storage-transmission: when there is an opportunity to offload data to earth stations, satellites directly transmit the data stored on the satellites to earth stations; (2) storage-relay-transmission: when data cannot be offloaded to earth stations, satellites can assist in data offloading by transmitting the data to the relay. The two transmission modes are shown in Fig. 1 by the blue solid line and the blue dotted line, respectively. Furthermore, due to the orbiting movements, the ISCR is time-varying, and the connection relationship between the satellite and the earth station is also time-varying. We assume that the network topology is quasi-static, i.e., the network topology is fixed in the time slot and changes between different time slots.

According to the link establishment rules of actual satellite systems [27], we consider a widely adopted inter-satellite link (ISL) connecting mode, i.e., "one-satellite four-chain" mode [28], to establish ISL in the intra-domain. Specifically, taking the  $D_1$  as an example, for  $cs_{ij}$ , the intra-plane ISL connections are established by connecting to  $cs_{i(j-1)}$  and  $cs_{i(j+1)}$ , and the inter-plane ISL connections are established by connecting to  $cs_{(i-1)j}$  and  $cs_{(i+1)j}$ . Furthermore, each satellite selects a satellite closest to itself to establish the inter-domain link (IDL) in each auxiliary domain. According to the above link establishment modes, each satellite determines the satellite that establishes an ISL as a relay assisting it to transmit data and the satellite that establishes an IDL as a relay assisting it to transmit data<sup>2</sup>. An example of the relays assisting data transmission is shown in Fig. 1. The set of relays assisting  $v_{ij}(D_k)$  to transmit data is represented as  $\mathcal{R}_{ij}(D_k, D_{k'})$ , where  $k' \in \{1, 2, 3\}$  is the index of domains. If  $k = k'$ ,  $\mathcal{R}_{ij}(D_k, D_{k'})$  represents the set of the intra-domain relays in  $D_k$  assisting  $v_{ij}(D_k)$  to transmit data and otherwise  $\mathcal{R}_{ij}(D_k, D_{k'})$  represents the set of the inter-domain relays in  $D_{k'}$  assisting  $v_{ij}(D_k)$  to transmit data. The connection relationship of ISLs/IDLs is represented as  $l_{ij}^t(D_k, m)$ , where  $m \in \mathcal{R}_{ij}(D_k, D_{k'})$  is the relays. For the satellite-ground link (SGL), since there is a limited number of transceivers at satellites, we assume that each satellite can only establish a transmission link with an earth station in each time slot. The connection relationship of SGL is represented as  $l_{ij}^t(D_k, es_g)$ ,

<sup>1</sup>When the satellite assists other satellites to transmit data, the satellite plays the role of a relay, which is referred to as a "relay" in this paper.

<sup>2</sup>In our model, satellites are equipped with receiving and transmitting antennas in pairs, and each satellite adopts the full-duplex mode. Furthermore, according to the rule of determining relays, each satellite can receive data transmitted by six satellites at most at the same time.

Table I  
THE KEY ABBREVIATIONS AND NOTATIONS.

Abbreviations/Symbols	Full name/Definition	Abbreviations/Symbols	Full name/Definition
RUR	Resource utilization ratio	CDRS	Cross-domain resource scheduling
HSRR	Hierarchical sparse resource representation	MDP	Markov decision problem
CD-DMRS	Cross-domain dynamic multi-resource scheduling	ISCR	Inter-satellite connection relationship
SOFM	Satellite orbit feature matrix	DNN	Deep neural network
MARL	Multi-agent reinforcement learning	RUE	Resource utilization efficiency
SSG	Snapshot sequence graph	TEG	Time-expanded graph
STAG	Storage time aggregated graph	ISL	Inter-satellite link
IDL	Inter-domain link	SGL	Satellite-ground link
ADTD	Amount of downloaded transmitted data	VBM	Visibility basis matrix
GICS	Geocentric inertial coordinate system	OPCS	Orbit plane coordinate system
A2C	Advantage actor-critic	TD	Temporal-difference
NCD-DMRS	Non-CD-DMRS	IA2C	Independent A2C
EDQN	Extended deep Q-network	FTS	Fair transmission selection
CRUE	Communication resource utilization efficiency	ERUE	Energy resource utilization efficiency
$\mathcal{I}_1, \mathcal{I}_2, \mathcal{I}_3$	The number of orbit in $D_1/D_2/D_3$	$\mathcal{J}_1, \mathcal{J}_2, \mathcal{J}_3$	The number of satellite in each orbit in $D_1/D_2/D_3$
$\mathcal{R}_{ij}(D_k, D_{k'})$	The set of relays of $v_{ij}(D_k)$	$l_{ij}^t(D_k, m), l_{ij}^t(D_k, es_g)$	The connection relationship of ISLs/IDLs/SGLs
$Cs_{ij}^t(D_k, m), Ce_{ij}^t(D_k, es_g)$	The achievable transmission rate of ISL/IDL/SGL	$o_{ij}^t(D_k)$	The data volume that can be collected/generated by $v_{ij}(D_k)$
$Ts_{ij}^t(D_k, m), Ts_{ij}^t(D_k, es_g)$	The data volume that can be transmitted from $v_{ij}(D_k)$ to its relays/es <sub>g</sub>	$u_{ij}^t(D_k, m), u_{ij}^t(D_k, es_g)$	Indicate whether the links from $v_{ij}(D_k)$ to its relays/es <sub>g</sub> are used
$E_{ijt}^t(D_k), E_{ijr}^t(D_k), E_{ijo}^t(D_k), E_{ijh}^t(D_k)$	The energy consumption of transmitting, receiving, and basic operation and the harvested energy by $v_{ij}(D_k)$	$Rs_{ij}^t(D_k), Ts_{ij}^t(D_k)$	The data volume than can be received/transmitted by $v_{ij}(D_k)$
$B_{max}, E_{max}, E_{min}$	The storage capacity, energy capacity, and the minimum residual energy of the battery	$s_{ij}^t(D_k), a_{ij}^t(D_k), r_{ij}^t(D_k)$	The state, action, and reward of $v_{ij}(D_k)$ in t-th time slot

where  $g = \{1, 2, \dots, N_{es}\}$  is the index of earth stations.

### B. Channel Model

In this subsection, the channel models of ISL/IDL and SGL are designed, to characterize the effect of channel changes on the transmission rate<sup>3</sup>.

1) *ISL/IDL Channel Model*: The achievable transmission rate of ISL/IDL from  $v_{ij}(D_k)$  to its relay in the t-th time slot is shown as follows [29], [30]:

$$Cs_{ij}^t(D_k, m) = \frac{P_{sst} G_{tr}^{ij}(D_k) G_{re}^m \mathcal{L}_{ij}^t(D_k, m)}{\mathcal{K} \mathcal{T} \cdot (E_b/N_0)_{req} \cdot \mathcal{M}}, \quad (1)$$

where the free space loss  $\mathcal{L}_{ij}^t(D_k, m)$  is

$$\mathcal{L}_{ij}^t(D_k, m) = \left( \frac{c}{4\pi \cdot Sl_{ij}^t(D_k, m) \cdot \mathcal{F}} \right)^2. \quad (2)$$

$P_{sst}$  is the constant transmission power of satellites for ISL/IDL.  $G_{tr}^{ij}(D_k)$  and  $G_{re}^m$  are the transmitting antenna gain and receiving antenna gain, respectively. Besides,  $\mathcal{K}$  and  $\mathcal{T}$  are the Boltzmann's constant and total system noise temperature.  $(E_b/N_0)_{req}$  and  $\mathcal{M}$  are the required ratio of received energy-per-bit to noise-density and link margin.  $Sl_{ij}^t(D_k, m)$  is the

<sup>3</sup>The channel capacity of ISL/IDL and SGL can be calculated using a unified practical engineering application formulation [29], and the Shannon formula is widely used for the calculation of SGL channel capacity. However, so far, in the research including ISL, the calculation method of the ISL channel capacity is rarely mentioned using the Shannon formula. Therefore, we still use the formula for the practical engineering application for calculation. Furthermore, we consider using non-overlapping frequency bands to effectively cancel the interference of multiple satellite transmissions.

slant range in the t-th time slot.  $c$  and  $\mathcal{F}$  are the speed of light and communication center frequency.  $Cs_{ij}^t(m, D_k)$  represents the achievable transmission rate of ISL/IDL from the other satellites to  $v_{ij}(D_k)$  in the t-th time slot.

2) *SGL Channel Model*: The Shannon formula is used to calculate the achievable transmission rate of SGL from  $v_{ij}(D_k)$  to  $es_g$  in the t-th time slot [31], denoted by  $Ce_{ij}^t(D_k, es_g)$ ,

$$Ce_{ij}^t(D_k, es_g) = \mathcal{B} \cdot \log_2 (1 + SNR_{ij}^t(D_k, es_g)), \quad (3)$$

where  $SNR_{ij}^t(D_k, es_g)$  is the *SNR* in the t-th time slot can be expressed as follows:

$$SNR_{ij}^t(D_k, es_g) = \frac{P_{set} G_{tr}^{ij}(D_k) G_{re}^g \mathcal{L}_{ij}^t(D_k, es_g) \mathcal{L}_p^t}{\mathcal{N}}. \quad (4)$$

$\mathcal{B}$  is the available transmission bandwidth.  $P_{set}$  is the constant transmission power of satellites for SGL.  $G_{re}^g$  is receiving antenna gain of  $es_g$ .  $\mathcal{L}_{ij}^t(D_k, es_g)$  is the free space loss, and  $\mathcal{L}_p^t$  is the propagation loss.  $\mathcal{N}$  is the noise.

### C. Data Arrival Model

Since the three domains have different functions and they need to complete the collection and transmission of different services, their data arrival characteristics are different. For  $D_1$ , we focus on the file transmission service, and since the user's transmission demands are differentiated, the data uploaded to communication satellites is random, and the data volume

is dynamic. According to [32], the arrival process of the traffic can be modeled as a Poisson process. The probability distribution of the number of arrivals in  $[t, t+1]$  can be written as

$$P(X_{ij}(D_1) = K) = \frac{e^{-\lambda_{ij}(D_1)} \cdot (\lambda_{ij}(D_1))^K}{K!}, K = 0, 1, \dots \quad (5)$$

where  $\lambda_{ij}(D_1)$  represents the data arrival rate and  $X_{ij}(D_1)$  is the number of arrivals during one time slot. Furthermore, although the data volume of the files that users need to transmit has certain differences, generally speaking, most of the files are small, and very few in large files. Therefore, the data volume of files can be approximately modeled by the exponential distribution [33]. The data volume that can be collected by  $cs_{ij}$  in  $t$ -th time slot, denoted by  $o_{ij}^t(D_1)$ , is defined as

$$o_{ij}^t(D_1) = \begin{cases} o_{ij}^t(D_1) \sim E(1/\rho_{ij}(D_1)), & \text{if data arrival,} \\ 0, & \text{else,} \end{cases} \quad (6)$$

where  $\rho_{ij}(D_1)$  is the average data volume uploaded.

For  $D_2$ , we focus on the transmission of observation service, and this service usually has a large data volume. Furthermore, due to the limited coverage of observation satellites, observation satellites do not have data arriving at every time slot. Whether the observation satellite can collect the observation data is predictable, and we can obtain the set of observation satellites that can collect the observation services in  $t$ -th time slot in advance  $V^t$ . The data volume that can be collected by  $os_{ij}$  in  $t$ -th time slot, denoted by  $o_{ij}^t(D_2)$ , is defined as

$$o_{ij}^t(D_2) = \begin{cases} \rho_{ij}(D_2), & \text{if } os_{ij} \in V^t, \\ 0, & \text{else,} \end{cases} \quad (7)$$

where  $\rho_{ij}(D_2)$  is the data volume observed by  $os_{ij}$ .

For  $D_3$ , we focus on the inter-satellite test data for navigation satellites to ensure the stability of the space-time benchmark, and the test data is downlinked and has a relatively small data volume. Since the test data is periodically generated, the arrival process of the traffic is modeled as the periodic arrival. The test data volume generated by  $ns_{ij}$  in  $t$ -th time slot, denoted by  $o_{ij}^t(D_3)$ , is defined as

$$o_{ij}^t(D_3) = \begin{cases} \rho_{ij}(D_3), & \text{if } t \bmod Td = 0, \\ 0, & \text{else,} \end{cases} \quad (8)$$

where  $\rho_{ij}(D_3)$  is the inter-satellite test data volume by  $ns_{ij}$  and  $Td$  is the data generation cycle.

Furthermore, we further clarify the differences among the quality of service (QoS) demands of different domains. Specifically, since the delay tolerance of the three types of services is significantly different, we focus on the delay demands of the three types of services. For example, the test data needs to be offloaded in time to ensure the validity of the data, and the observation data usually has a high delay tolerance. Furthermore, we quantify the delay demand into time slots and adopt the survival time slots to measure it, i.e., the higher

the delay tolerance, the greater the survival time slots<sup>4</sup>. The survival time slots are denoted by  $\mathcal{RS}(D_k)$ .

#### D. Energy Model

In this subsection, we present the energy model, including the energy consumption and harvesting model.

The energy consumption of  $v_{ij}(D_k)$  for transmitting data during  $t$ -th time slot.

$$\begin{aligned} E_{ijt}^t(D_k) = & \sum_{k'=1}^3 \sum_{m \in \mathcal{R}_{ij}(D_k, D_{k'})} P_{sst} \cdot \frac{T s_{ij}^t(D_k, m) \cdot u_{ij}^t(D_k, m)}{C s_{ij}^t(D_k, m)} \\ & + \sum_{g=1}^{N_{es}} P_{set} \cdot \frac{T s_{ij}^t(D_k, es_g) \cdot u_{ij}^t(D_k, es_g)}{C e_{ij}^t(D_k, es_g)}, \end{aligned} \quad (9)$$

where  $T s_{ij}^t(D_k, m)$  is the data volume that can be transmitted from  $v_{ij}(D_k)$  to its relay, and  $T s_{ij}^t(D_k, es_g)$  is the data volume that can be transmitted from  $v_{ij}(D_k)$  to  $es_g$ .  $u_{ij}^t(D_k, m)$  and  $u_{ij}^t(D_k, es_g) \in \{0, 1\}$  respectively indicate whether the links from  $v_{ij}(D_k)$  to its relay or  $es_g$  are used, 1 if used and 0 otherwise. It should be noted that due to the limitations of the link capacity, the data volume stored, and the battery energy,  $T s_{ij}^t(D_k, m) \leq \min(C s_{ij}^t(D_k, m) \cdot \tau, B_{ij}^{t-1}(D_k))$  and  $T s_{ij}^t(D_k, es_g) \leq \min(C e_{ij}^t(D_k, es_g) \cdot \tau, B_{ij}^{t-1}(D_k))$ .  $B_{ij}^{t-1}(D_k)$  is the data volume stored in  $v_{ij}(D_k)$  at the end of  $t-1$ -th time slot.

We denote  $E_{ijr}^t(D_k)$  as energy consumption of  $v_{ij}(D_k)$  for receiving data during  $t$ -th time slot.  $E_{ijr}^t(D_k)$  is shown as follows:

$$E_{ijr}^t(D_k) = \frac{R s_{ij}^t(D_k)}{(S s_{ij}^t(D_k))_{max}} \cdot P_{sr} \cdot \tau \cdot U_{ij}^t(D_k), \quad (10)$$

where  $(S s_{ij}^t(D_k))_{max}$  is the total link capacity of used links transmitting data to  $v_{ij}(D_k)$ , denoted by

$$(S s_{ij}^t(D_k))_{max} = \left( \sum_{k'=1}^3 \sum_{m \in \mathcal{R}_{ij}(D_k)} C s_{ij}^t(m, D_k) \cdot u_{ij}^t(m, D_k) \right) \cdot \tau, \quad (11)$$

and  $R s_{ij}^t(D_k) = \min(S s_{ij}^t(D_k), D_{ijr}^t(D_k))$  is the data volume that can be received by  $v_{ij}(D_k)$ .  $\mathcal{R}_{ij}(D_k) = \{v_{i'j'}(D_{k'}) | v_{ij}(D_k) \in \mathcal{R}_{i'j'}(D_{k'}, D_k), i' \in \{1, 2, \dots, I_{k'}\}, j' \in \{1, 2, \dots, J_{k'}\}\}$  is the set of satellites transmitting data to  $v_{ij}(D_k)$ .  $S s_{ij}^t(D_k)$  is the total data volume transmitted to  $v_{ij}(D_k)$  and  $D_{ijr}^t(D_k)$  is the maximum data volume that can be received by  $v_{ij}(D_k)$ <sup>5</sup>.  $P_{sr}$  is the reception power of satellites.  $U_{ij}^t(D_k)$  is the number of receivers activated by  $v_{ij}(D_k)$ .

Moreover, we use  $E_{ijo}^t(D_k)$  to denote the energy consumption of  $v_{ij}(D_k)$  for basic operation during  $t$ -th time slot.  $E_{ijo}^t(D_k)$  can be expressed as

$$E_{ijo}^t(D_k) = P_o \cdot \tau, \quad (12)$$

where  $P_o$  is the basic operation power.

<sup>4</sup>The survival time slots are decremented during the scheduling, and the remaining survival time slots are different in each time slot. Furthermore, data can only be successfully offloaded during the survival time slot, and the time-out data will be deleted, i.e., the remaining survival time slot is zero.

<sup>5</sup>The formulations of  $S s_{ij}^t(D_k)$  and  $D_{ijr}^t(D_k)$  are shown in Section IV-C.

The total energy consumption of  $v_{ij}(D_k)$  during  $t$ -th time slot, denoted by  $E_{ijc}^t(D_k)$ , consisted of the above three energy consumption items and is shown as

$$E_{ijc}^t(D_k) = E_{ijt}^t(D_k) + E_{ijr}^t(D_k) + E_{ijo}^t(D_k). \quad (13)$$

We denote  $E_{ijh}^t(D_k)$  as the harvested energy of  $v_{ij}(D_k)$  over the  $t$ -th time slot, which can be determined in advance based on orbital dynamics. In addition, we assume that the on-board battery has a causal relationship, so the energy harvested in the  $t$ -th time slot is not observed when the action of the  $t$ -th time slot is performed.  $E_{ijh}^t(D_k)$  can be expressed as follows

$$E_{ijh}^t(D_k) = P_h \cdot \min \{ \tau, y_{ij}^t(D_k) \}, \quad (14)$$

where  $P_h$  is the energy collection rate.  $y_{ij}^t(D_k)$  is the duration that  $v_{ij}(D_k)$  is covered by the sun at the beginning of the  $t$ -th time slot.

### E. Problem Formulation

In our work, we aim to maximize the total amount of downloaded transmitted data (ADTD) in the planning cycle while satisfying QoS demands and the constraints of communication, storage, and energy resources. Resource constraints are as follows:

- Communication resource constraint: Due to the limited transmission rate of ISL/IDL and SGL, the total data transmission volume of each satellite cannot be violated,

$$Ts_{ij}^t(D_k) \leq \left( \sum_{k'=1}^3 \sum_{m \in \mathcal{R}_{ij}(D_k, D_{k'})} Cs_{ij}^t(D_k, m) \cdot u_{ij}^t(D_k, m) + \sum_{g=1}^{N_{es}} Ce_{ij}^t(D_k, es_g) \cdot u_{ij}^t(D_k, es_g) \right) \cdot \tau, \quad (15)$$

where  $Ts_{ij}^t(D_k)$  is the data volume that can be transmitted by  $v_{ij}(D_k)$ , denoted by

$$Ts_{ij}^t(D_k) = \sum_{k'=1}^3 \sum_{m \in \mathcal{R}_{ij}(D_k, D_{k'})} Ts_{ij}^t(D_k, m) \cdot u_{ij}^t(D_k, m) + \sum_{g=1}^{N_{es}} Ts_{ij}^t(D_k, es_g) \cdot u_{ij}^t(D_k, es_g). \quad (16)$$

- Storage resource constraint: The amount of data stored on the satellite cannot exceed the specified limit, i.e.,

$$B_{ij}^{t-1}(D_k) + o_{ij}^t(D_k) + Rs_{ij}^t(D_k) - Ts_{ij}^t(D_k) \leq B_{max}, \quad (17)$$

where  $B_{max}$  is the storage capacity.

- Energy resource constraint: Similarly, the battery capacity of the satellite is limited, and all energy cannot be fully used for data transmission and reception to maintain the normal operation of the satellite in the shadow,

$$E_{ij}^{t-1}(D_k) - E_{ijc}^t(D_k) \geq E_{min}, \quad (18)$$

where  $E_{ij}^{t-1}(D_k)$  is the residual energy in  $v_{ij}(D_k)$  at the end of  $t-1$ -th time slot,  $E_{min} = (1-\eta) \cdot E_{max}$  is the minimum residual energy of the battery,  $\eta$  is the maximum discharge depth of the battery, and  $E_{max}$  is the

battery capacity. Meanwhile, the battery energy cannot exceed the battery capacity,

$$E_{ij}^{t-1}(D_k) + \widetilde{E_{ijh}^t}(D_k) - E_{ijc}^t(D_k) \leq E_{max}, \quad (19)$$

where  $\widetilde{E_{ijh}^t}(D_k) \leq E_{ijh}^t(D_k)$  is the actual harvested energy. The reason is that during the energy harvesting process, if the battery energy reaches the battery capacity, the satellite is not continuing harvesting energy during the remaining time covered by the sun.

In addition, each satellite can only select one link for data transmission in each time slot, i.e., only one link can be used,

$$\sum_{k'=1}^3 \sum_{m \in \mathcal{R}_{ij}(D_k, D_{k'})} u_{ij}^t(D_k, m) + \sum_{g=1}^{N_{es}} u_{ij}^t(D_k, es_g) = 1. \quad (20)$$

According to the above constraints, we formulate the CDRS problem to maximize the total ADTD.

$$\begin{aligned} \text{CDRS: } & \max_{\substack{u_{ij}^t(D_k, m), k \in \{1, 2, 3\} \\ u_{ij}^t(D_k, es_g)}} \sum_{k=1}^3 D(D_k) \\ & \text{s.t. (15)} - (20), \end{aligned} \quad (21)$$

where  $D(D_k) = \sum_{i=1}^{I_k} \sum_{j=1}^{J_k} \sum_{t=1}^T \sum_{g=1}^{N_{es}} Ts_{ij}^t(D_k) \cdot u_{ij}^t(D_k, es_g)$  is the ADTD of  $D_k$ .

CDRS problem is an integer programming problem, which belongs to the NP-hard problem, and service demands are dynamic, which leads to high solution complexity. In addition, to solve the CDRS problem directly, it is inevitable to need to characterize the ISCRs of all time slots of the whole network in advance, which leads to high space complexity of communication resource representation. Therefore, we propose an HSRR scheme to realize the real-time representation of communication resources, and solve the CDRS problem by equivalent conversion.

## IV. SPARSE REPRESENTATION AND CDRS PROBLEM EQUIVALENT CONVERSION

In this section, we first analyze the periodicity of the ISCR in the same layer and use the property to design an intra-layer sparse representation scheme according to the motion law of satellites. Then, we explore the orbit motion characteristics of satellites and design an inter-layer sparse representation scheme by constructing the SOFM of each domain. Intra-layer sparse representation and inter-layer sparse representation jointly realize the HSRR<sup>6</sup>. Furthermore, we analyze the space complexity of the two schemes. Finally, based on the HSRR, we convert the CDRS problem to the MDP.

### A. Hierarchical Sparse Resource Representation

1) *Intra-Layer Sparse Representation*: Due to the orbiting movements, the satellites at the same orbit altitude have the same operation cycle, which makes the connection relationship periodic between satellites in the intra-layer and can be repeated periodically in a short time. Therefore, we only need

<sup>6</sup>Since there is usually a stable connection between satellites in the same orbit, we mainly focus on the sparse characteristics between satellites in different orbits.

to obtain the ISCRs of one cycle and obtain the ISCR of any time slot by periodic extension.

Specifically, we first binarize the ISCRs of one cycle. If there is a connection relationship between two satellites, set  $l_{ij}^t(D_k, m) = 1$ , i.e., there is visibility between the two satellites. Otherwise, set  $l_{ij}^t(D_k, m) = 0$ . According to the above processing rules, a visibility basis matrix (VBM) is obtained, denoted by  $L_{ij}(D_k, m) = [l_{ij}^{t_{sta}}(D_k, m), l_{ij}^{t_{sta}+1}(D_k, m), \dots, l_{ij}^{t_{end}}(D_k, m)]$ , where  $t_{sta}$  is the start slot and  $t_{end}$  is the end slot of the first complete cycle. For any time slot  $t$ :

$$l_{ij}^t(D_k, m) = \begin{cases} l_{ij}^{\Gamma_{ij}(D_k, m)+t}(D_k, m), & \text{if } t < t_{sta}, \\ l_{ij}^t(D_k, m), & \text{if } t_{sta} \leq t \leq t_{end}, \\ l_{ij}^{((t-t_{sta}) \bmod \Gamma_{ij}(D_k, m) + t_{sta}-1)}(D_k, m), & \text{if } t > t_{end}, \end{cases} \quad (22)$$

where  $m \in \mathcal{R}_{ij}(D_k, D_{k'})$ ,  $k = k'$ , and  $\Gamma_{ij}(D_k, m) \in \{1, 2, \dots, T\}$  is the cycle of the connection relationship between  $v_{ij}(D_k)$  and its relay of intra-domain. Further, the VBMs that satisfy the rotational closure [34] are divided into a representation group  $G_f(D_k)$  ( $f \in \{1, 2, \dots, F_k\}$ ,  $F_k \leq (\mathcal{I}_k \cdot \mathcal{J}_k)$ ).  $G_f(D_k)$  selects a VBM as the rotation basis matrix  $L_f(D_k)$ , and according to the  $L_f(D_k)$ , we obtain the rotation distances  $\Delta d_{ij}^f(D_k, m)$  of other VBMs in the  $G_f(D_k)$  relative to the  $L_f(D_k)$ . Then,  $l_{ij}^t(D_k, m)$  is rewritten as

$$l_{ij}^t(D_k, m) = \begin{cases} l_{ij}^{(\Gamma_f(D_k)+t+\Delta d_{ij}^f(D_k, m)) \bmod T}(D_k, m), & \text{if } t < t_{sta}, \\ l_{ij}^{(t+\Delta d_{ij}^f(D_k, m)) \bmod T}(D_k, m), & \text{if } t_{sta} \leq t \leq t_{end}, \\ l_{ij}^{((t-t_{sta}) \bmod \Gamma_f(D_k) + t_{sta}-1 + \Delta d_{ij}^f(D_k, m)) \bmod T}(D_k, m), & \text{if } t > t_{end}, \end{cases} \quad (23)$$

If there is only a VBM in the group,  $\Delta d_{ij}^f(D_k, m) = 0$  and (23) degenerates to (22).

When characterizing the ISCRs in the intra-layer, we use  $L_f(D_k)$  and the rotation distance matrix  $\Delta d_f(D_k)$  to characterize the ISCRs of all time slots and can obtain the ISCR of any time slot according to (23), which can reduce the space complexity of communication resource representation, and with the increase of the planning cycle, the advantage of the intra-layer sparse representation will become more and more obvious.

2) *Inter-Layer Sparse Representation*: For different orbit altitudes, since the orbit operation cycles are different, it becomes very difficult for the ISCR to repeat periodically in a short time. Therefore, the communication resource representation scheme of intra-layer satellites can not be directly applied to inter-layer satellites. In order to solve the problem and avoid resulting in too high space complexity, we start from the orbit motion characteristics, construct the SOFM of each domain, and use the SOFMs to deduce the network topology among domains to realize the real-time representation of the ISCR of inter-layer satellites.

SOFM consists of satellite orbit parameters in the initial

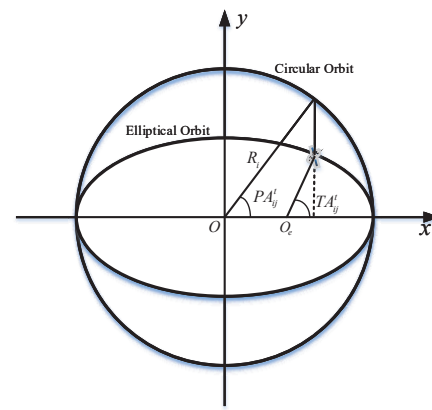


Figure 2. Geometric relationship between true anomaly and eccentric anomaly.

time slot<sup>7</sup>, and SOFM is expressed as

$$OF(D_k)=$$

$$\begin{bmatrix} h_1 & e_1 & I_1 & \Omega_1 & RA_1 & \overline{TA_{11}^1} & \dots & \overline{TA_{1j}^1} & \dots & \overline{TA_{1\mathcal{J}_k}^1} \\ \vdots & \vdots & \vdots & \vdots & \vdots & \vdots & \dots & \vdots & \dots & \vdots \\ h_i & e_i & I_i & \Omega_i & RA_i & \overline{TA_{i1}^1} & \dots & \overline{TA_{ij}^1} & \dots & \overline{TA_{i\mathcal{J}_k}^1} \\ \vdots & \vdots & \vdots & \vdots & \vdots & \vdots & \dots & \vdots & \dots & \vdots \\ h_{\mathcal{I}_k} & e_{\mathcal{I}_k} & I_{\mathcal{I}_k} & \Omega_{\mathcal{I}_k} & RA_{\mathcal{I}_k} & \overline{TA_{\mathcal{I}_k 1}^1} & \dots & \overline{TA_{\mathcal{I}_k j}^1} & \dots & \overline{TA_{\mathcal{I}_k \mathcal{J}_k}^1} \end{bmatrix},$$

where  $h_i$  is the orbit height,  $e_i$  is eccentricity,  $I_i$  is inclination,  $\Omega_i$  is argument of perigee,  $RA_i$  is right ascension of ascending node,  $TA_{ij}^1$  is mean anomaly in the first time slot,  $i \in \{1, 2, \dots, \mathcal{I}_k\}$ ,  $j \in \{1, 2, \dots, \mathcal{J}_k\}$ . When characterizing the communication resources of inter-layer satellites, we obtain the position information of the satellites by looking up the SOFM and use the information to judge whether a link can be established between the satellites. Specifically, it mainly includes two parts: (1) Obtain the coordinates of satellites in J2000.0 geocentric inertial coordinate system (GICS):

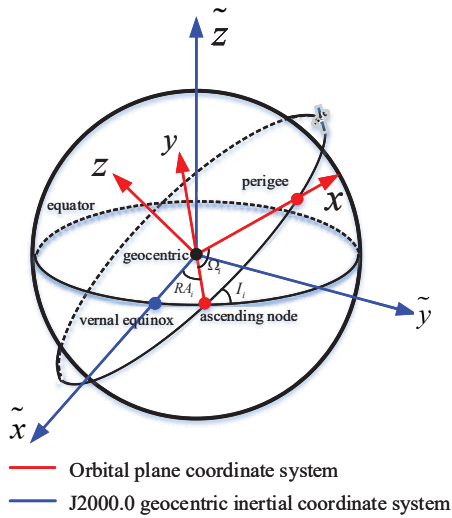
$$\begin{bmatrix} \widetilde{x_{ij}^t}(D_k) \\ \widetilde{y_{ij}^t}(D_k) \\ \widetilde{z_{ij}^t}(D_k) \end{bmatrix} = M(\Omega_i) \cdot M(I_i) \cdot M(RA_i) \cdot \begin{bmatrix} x_{ij}^t(D_k) \\ y_{ij}^t(D_k) \\ z_{ij}^t(D_k) \end{bmatrix}, \quad (24)$$

where  $\begin{bmatrix} \widetilde{x_{ij}^t}(D_k) & \widetilde{y_{ij}^t}(D_k) & \widetilde{z_{ij}^t}(D_k) \end{bmatrix}^T$  is the coordinate of  $v_{ij}(D_k)$  in J2000.0 GICS,  $\begin{bmatrix} x_{ij}^t(D_k) & y_{ij}^t(D_k) & z_{ij}^t(D_k) \end{bmatrix}^T$  is the coordinate of  $v_{ij}(D_k)$  in  $i$ -th orbit plane coordinate system (OPCS),

$$\begin{bmatrix} x_{ij}^t(D_k) \\ y_{ij}^t(D_k) \\ z_{ij}^t(D_k) \end{bmatrix} = \widetilde{R_{ij}(D_k)} \cdot \left( \cos(TA_{ij}^t) \cdot \begin{bmatrix} 1 \\ 0 \\ 0 \end{bmatrix} + \sin(TA_{ij}^t) \cdot \begin{bmatrix} 0 \\ 1 \\ 0 \end{bmatrix} \right), \quad (25)$$

where  $\widetilde{R_{ij}(D_k)} = R_i \cdot (1 - e_i \cdot \cos(PA_{ij}^t))$  is the true distance from  $v_{ij}(D_k)$  to the center of mass of the earth,  $R_i = R_e + h_i$  is orbit radius,  $R_e$  is the earth radius,  $PA_{ij}^t$  is the eccentric anomaly and can be obtained through iteration, the iterative formula is

<sup>7</sup>In this paper, we consider the TwoBody model, so the orbit height, eccentricity, inclination, argument of perigee, and right ascension of ascending node are constant during the satellite operation. However, mean anomaly is constantly changing with the movement of the satellite.



$$PA_{ij}^t(n+1) = \overline{TA}_{ij}^t + e_i \cdot \sin(PA_{ij}^t(n)), \quad (26)$$

where the iterative initial value is set that  $PA_{ij}^t(0) = \overline{TA}_{ij}^t$ , convergence condition is  $|PA_{ij}^t(n+1) - PA_{ij}^t(n)| < \xi$ ,  $\xi$  is accuracy.  $\overline{TA}_{ij}^t$  is mean anomaly in  $t$ -th time slot

$$\overline{TA}_{ij}^t = \overline{TA}_{ij}^1 + \omega_i \cdot (t-1) \cdot \tau, \quad (27)$$

where  $\omega_i = \sqrt{\frac{GM}{R_i^3}}$  is the angular velocity,  $G$  is the gravitational constant, and  $M$  is the mass of the earth.  $TA_{ij}^t$  is true anomaly, when the orbit is circular, i.e.,  $e_i = 0$ ,  $TA_{ij}^t = \overline{TA}_{ij}^t$ , when the orbit is elliptical, i.e.,  $e_i \neq 0$ ,

$$TA_{ij}^t = \arctan \left( \frac{\sqrt{1-e_i^2} \cdot \sin(PA_{ij}^t)}{\cos(PA_{ij}^t) - e_i} \right). \quad (28)$$

Geometric relationship between true anomaly and eccentric anomaly is shown in Fig. 2, where  $O_e$  is the center of mass of the earth.  $M(\Omega_i)$ ,  $M(I_i)$  and  $M(RA_i)$  are  $3 \times 3$  matrices, respectively and are expressed as

$$M(\Omega_i) = \begin{bmatrix} \cos(\Omega_i) & \sin(\Omega_i) & 0 \\ -\sin(\Omega_i) & \cos(\Omega_i) & 0 \\ 0 & 0 & 1 \end{bmatrix},$$

$$M(I_i) = \begin{bmatrix} 1 & 0 & 0 \\ 0 & \cos(I_i) & \sin(I_i) \\ 0 & -\sin(I_i) & \cos(I_i) \end{bmatrix},$$

$$M(RA_i) = \begin{bmatrix} \cos(RA_i) & \sin(RA_i) & 0 \\ -\sin(RA_i) & \cos(RA_i) & 0 \\ 0 & 0 & 1 \end{bmatrix}.$$

The establishment method of the two coordinate systems is shown in Fig. 3, where the red solid line represents the OPCS, and the blue solid line represents the J2000.0 GICS. (2) Determine the ISCR: Due to the occlusion of the earth,  $v_{ij}(D_k)$  and  $v_{ij}(D_{k'})$  ( $k \neq k'$ ) have the maximum visible distance, i.e., line of sight. We assume that  $v_{ij}(D_k)$  and  $v_{ij}(D_{k'})$

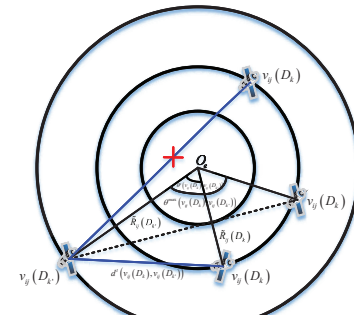


Figure 4. Satellite link establishment in the circular orbit.

can communicate normally within the line of sight, and use the maximum geocentric angle  $\theta^{max}(v_{ij}(D_k), v_{ij}(D_{k'}))$  between  $v_{ij}(D_k)$  and  $v_{ij}(D_{k'})$  as the benchmark to determine whether  $v_{ij}(D_k)$  and  $v_{ij}(D_{k'})$  have visibility. As shown in Fig. 4, the blue solid line indicates that  $v_{ij}(D_k)$  and  $v_{ij}(D_{k'})$  want to establish a link, and the red "x" indicates that there is no visibility between  $v_{ij}(D_k)$  and  $v_{ij}(D_{k'})$ .  $\theta^{max}(v_{ij}(D_k), v_{ij}(D_{k'}))$  can be expressed as

$$\theta^{max}(v_{ij}(D_k), v_{ij}(D_{k'})) = \arccos\left(\frac{R_e}{R_{ij}(D_k)}\right) + \arccos\left(\frac{R_e}{R_{ij}(D_{k'})}\right). \quad (29)$$

Geocentric angle  $\theta^t(v_{ij}(D_k), v_{ij}(D_{k'}))$  between  $v_{ij}(D_k)$  and  $v_{ij}(D_{k'})$  in  $t$ -th time slot can be expressed as in (30), where  $d^t(v_{ij}(D_k), v_{ij}(D_{k'}))$  is the distance between  $v_{ij}(D_k)$  and  $v_{ij}(D_{k'})$ , expressed as in (31). If  $\theta^t(v_{ij}(D_k), v_{ij}(D_{k'})) \leq \theta^{max}(v_{ij}(D_k), v_{ij}(D_{k'}))$ , the link can be established. For  $v_{ij}(D_k)$  and its relay of inter-domain, if the link can be established between them,  $l_{ij}^t(D_k, m) = 1$ , where  $m \in \mathcal{R}_{ij}(D_k, D_{k'})$ ,  $k \neq k'$ . Otherwise,  $l_{ij}^t(D_k, m) = 0$ .

In this way, we do not need to store the ISCRs of all time slots in advance, but only the SOFM, which greatly reduces the space complexity of communication resource representation.

### B. Space Complexity Analysis of Representation

Taking  $D_1$  and  $D_2$  as an example to calculate the space complexity of representation, we first calculate the storage space occupied by the intra-layer sparse representation scheme. We assume that  $D_1$  and  $D_2$  consist of a single layer of satellites<sup>8</sup> and all satellites in the intra-domain establish links according to Section III-A. Furthermore, we consider the case that each representation group only has a VBM, and the storage space occupied at this time is the maximum. Since the connection relationship between any two satellites is different, and their visibility cycles are also different, we choose the maximum visibility cycle to calculate the space complexity, then  $C_{h1} = \mathcal{O}((\mathcal{I}_1 \cdot \mathcal{J}_1) \cdot \Gamma_1^{max} + (\mathcal{I}_2 \cdot \mathcal{J}_2) \cdot \Gamma_2^{max})$ , where  $\Gamma_1^{max}$  and  $\Gamma_2^{max}$  are maximum visibility cycle of  $D_1$  and  $D_2$  respectively.

<sup>8</sup>At this time, the intra-layer is the intra-domain, and the inter-layer is the inter-domain. Next, this paper adopts the intra-domain and inter-domain to describe.

$$\theta^t(v_{ij}(D_k), v_{ij}(D_{k'})) = \arccos \left( \frac{\left(\widetilde{R}_{ij}(D_k)\right)^2 + \left(\widetilde{R}_{ij}(D_{k'})\right)^2 - \left(d^t(v_{ij}(D_k), v_{ij}(D_{k'}))\right)^2}{2 \cdot \left(\widetilde{R}_{ij}(D_k)\right) \cdot \left(\widetilde{R}_{ij}(D_{k'})\right)} \right), \quad (30)$$

$$d^t(v_{ij}(D_k), v_{ij}(D_{k'})) = \sqrt{\left(\widetilde{x}_{ij}^t(D_k) - \widetilde{x}_{ij}^t(D_{k'})\right)^2 + \left(\widetilde{y}_{ij}^t(D_k) - \widetilde{y}_{ij}^t(D_{k'})\right)^2 + \left(\widetilde{z}_{ij}^t(D_k) - \widetilde{z}_{ij}^t(D_{k'})\right)^2}. \quad (31)$$

We also consider the above network for the inter-layer sparse representation scheme. According to the rules constructed by the SOFM, we only need to calculate the storage space occupied by the SOFM of each domain, then the space complexity is  $C_{h2} = \mathcal{O}((\mathcal{J}_1 + 5) \cdot \mathcal{I}_1 + (\mathcal{J}_2 + 5) \cdot \mathcal{I}_2)$ . The space complexity of the HSRR is  $C_{hsrr} = C_{h1} + C_{h2}$ .

TEG directly represents the ISCR of each time slot. The space complexity is  $C_{t1} = \mathcal{O}((\mathcal{I}_1 \cdot \mathcal{J}_1) + (\mathcal{I}_2 \cdot \mathcal{J}_2) \cdot T)$  in the intra-domain, and  $C_{t2} = \mathcal{O}((\mathcal{I}_1 \cdot \mathcal{J}_1) \cdot (\mathcal{I}_2 \cdot \mathcal{J}_2) \cdot T)$  in the inter-domain. The space complexity of the TEG is  $C_{teg} = C_{t1} + C_{t2}$ . There are thousands of satellites in satellite networks, so  $C_{hsrr} \approx \mathcal{O}((\mathcal{I}_1 \cdot \mathcal{J}_1) \cdot \Gamma_1^{max} + (\mathcal{I}_2 \cdot \mathcal{J}_2) \cdot \Gamma_2^{max})$  and  $C_{teg} \approx \mathcal{O}((\mathcal{I}_1 \cdot \mathcal{J}_1) \cdot (\mathcal{I}_2 \cdot \mathcal{J}_2) \cdot T)$ . Considering the extreme case, i.e.,  $\Gamma_1^{max} = \Gamma_2^{max} = T$ , the space complexity of communication resource representation is reduced from  $\mathcal{O}((\mathcal{I}_1 \cdot \mathcal{J}_1) \cdot (\mathcal{I}_2 \cdot \mathcal{J}_2) \cdot T)$  to  $\mathcal{O}((\mathcal{I}_1 \cdot \mathcal{J}_1) + (\mathcal{I}_2 \cdot \mathcal{J}_2) \cdot T)$ . It can be seen that the HSRR can effectively reduce the space complexity of communication resource representation for satellite networks. Further, we briefly analyze the computational complexity. On the one hand, the ISCR of the ISL/IDL required to be calculated for each satellite is constant, i.e., independent of the number of time slots, and the time required for calculation is compared with the time slot interval almost negligible. On the other hand, the time required for each satellite to calculate ISCR using HSRR in each time slot increases linearly with the number of ISL/IDL, which mainly depends on different link establishment rules. To sum up, compared with HSRR, which reduces the space complexity of representation, HSRR has a small cost in terms of computational complexity.

### C. CDRS Problem Equivalent Conversion

Due to the real-time representation of communication resources by HSRR, it is possible to perform global resource scheduling without obtaining all ISCRs in advance. Furthermore, since the goal of resource scheduling is to achieve the successful offloading of more data, the essence of resource scheduling is data transmission. The amount of received and transmitted data in the current time slot is independent of those in the past time slots. Therefore, we convert the CDRS problem to MDP to solve it.

In our model, we set the state  $s_{ij}^t(D_k)$  is represented by a 3-tuple, i.e.,

$$s_{ij}^t(D_k) = \left(B_{ij}^{t-1}(D_k), E_{ij}^{t-1}(D_k), \overline{\mathcal{RS}}_{ij}^{t-1}(D_k)\right), \quad (32)$$

where  $B_{ij}^{t-1}(D_k)$  is any value in a continuous range of  $[0, B_{max}]$ .  $E_{ij}^{t-1}(D_k)$  is any value in a continuous range of

$[0, E_{max}]$ .  $\overline{\mathcal{RS}}_{ij}^{t-1}(D_k)$  is the average remaining survival time slots of data stored in  $v_{ij}(D_k)$  at the end of  $t-1$ -th time slot.  $B_{ij}^t(D_k)$  can be expressed as

$$B_{ij}^t(D_k) = B_{ij}^{t-1}(D_k) + o_{ij}^t(D_k) + R_{ij}^t(D_k) - T s_{ij}^t(D_k). \quad (33)$$

In the  $R s_{ij}^t(D_k)$ ,  $S s_{ij}^t(D_k)$  is denoted by

$$S s_{ij}^t(D_k) = \sum_{k'=1}^3 \sum_{m \in \mathbb{R}_{ij}(D_k)} T s_{ij}^t(m, D_k) \cdot u_{ij}^t(m, D_k), \quad (34)$$

and  $D_{ijr}^t(D_k)$  is expressed as in (35), where  $C s_{ij}^t(D_k) = (S s_{ij}^t(D_k))_{max}/\tau$  is the total receive rate by  $v_{ij}(D_k)$ .  $B_{ijr}^t(D_k) = B_{max} - (B_{ij}^{t-1}(D_k) - T s_{ij}^t(D_k))$  is the residual storage capacity.  $E_{ij}^t(D_k)$  can be expressed as

$$E_{ij}^t(D_k) = E_{ij}^{t-1}(D_k) + \widetilde{E}_{ijh}^t(D_k) - E_{ijc}^t(D_k). \quad (36)$$

The available action set of  $v_{ij}(D_k)$  corresponds to its relays and the earth station that can be selected, then  $A_{ij}^t(D_k) = \{a_{ij}^t(D_k) = p | l_{ij}^t(D_k, p) = 1, p \in \{\mathcal{R}_{ij}(D_k, D_{k'}) | k' = \{1, 2, 3\}\} \cup v_{ij}(D_k)\}$ , where  $v_{ij}(D_k)$  is used to indicate that the data is transmitted to the earth station, if  $\exists l_{ij}^t(D_k, es_g) = 1$ ,  $l_{ij}^t(D_k, v_{ij}(D_k)) = 1$ , otherwise  $l_{ij}^t(D_k, v_{ij}(D_k)) = 0$ .

Since the satellites affect each other when transmitting data, we consider a multi-agent network scenario in order to achieve efficient resource scheduling of the whole network. Moreover, we use local state information to make a decision. The reason lies in that the impact of relays of satellites on the state is the most important, and with the increase of network scale, it is infeasible to obtain the state information of all satellites in real-time [35]. The local state information is

$$S_{ij}^t(D_k) = s_{ij}^t(D_k) \cup [s_m^t]_{m \in \{\mathcal{R}_{ij}(D_k, D_{k'}) | k' = \{1, 2, 3\}\}}, \quad (37)$$

where  $s_m^t$  represents the state of relay of  $v_{ij}(D_k)$ .

The reward consists of two parts: (1) We set the data volume transmitted as the profit value, expressed as in (38), where  $\delta_{ij}(D_k)$  is the advantage factor to measure the resource supply capability of each domain.  $\zeta_{ij}(D_k, m)$  is the supply-demand relationship factor to describe the difference of the data demands and resource supply for the transmitting and receiving satellites. (2) In order to reduce the loss caused by insufficient memory or battery energy of the receiving satellite, a penalty mechanism is introduced. The mean of the loss data amount is used as the penalty value

$$p u_{ij}^t(D_k) = \frac{\max(S s_{a_{ij}^t}^t(D_k) - R s_{a_{ij}^t}^t(D_k), 0)}{U_{a_{ij}^t}^t(D_k)}, \quad (39)$$

$$D_{ijr}^t(D_k) = \begin{cases} \min \left( \min \left( \frac{E_{ij}^{t-1}(D_k) - E_{ijt}^t(D_k) - E_{min}}{U_{ij}^t(D_k) \cdot P_{sr}}, \tau \right), C s_{ij}^t(D_k), B_{ijr}^t(D_k) \right), & \text{if } (E_{ij}^{t-1}(D_k) - E_{ijt}^t(D_k)) \geq E_{min}, \\ 0, & \text{else,} \end{cases} \quad (35)$$

$$pr_{ij}^t(D_k) = \delta_{ij}(D_k) \cdot \left( \sum_{g=1}^{N_{es}} T s_{ij}^t(D_k, es_g) \cdot u_{ij}^t(D_k, es_g) + \sum_{k'=1, k' \neq k}^3 \sum_{m \in \mathcal{R}_{ij}(D_k, D_{k'})} \zeta_{ij}(D_k, m) \cdot T s_{ij}^t(D_k, m) \cdot u_{ij}^t(D_k, m) \right), \quad (38)$$

### Algorithm 1 Relays Selection Algorithm

**Input:**  $\mathcal{I}_1, \mathcal{J}_1, \mathcal{I}_2, \mathcal{J}_2, \mathcal{I}_3, \mathcal{J}_3$ .

- 1: set  $t = 1$ .
- 2: **for**  $k \in \{1, 2, 3\}$  **do**
- 3:   **for**  $i \in \{1, 2, \dots, \mathcal{I}_k\}$  **do**
- 4:     **for**  $j \in \{1, 2, \dots, \mathcal{J}_k\}$  **do**
- 5:       get coordinates of the satellite  $(\tilde{x}_{ij}^t(D_k), \tilde{y}_{ij}^t(D_k), \tilde{z}_{ij}^t(D_k))$ .
- 6:       get coordinates of all satellites of auxiliary domains  $(\tilde{x}_{ij}^t(D_{k'}), \tilde{y}_{ij}^t(D_{k'}), \tilde{z}_{ij}^t(D_{k'}))$ ,  $(k' \in \{1, 2, 3\} \cap k' \neq k)$ .
- 7:       calculate the distance  $d^t(v_{ij}(D_k), v_{ij}(D_{k'}))$ .
- 8:       select  $\arg \min(d^t(v_{ij}(D_k), v_{ij}(D_{k'})))$  in each auxiliary domain as the relay of  $v_{ij}(D_k)$ ,  $(k' \in \{1, 2, 3\} \cap k' \neq k)$ .
- 9:     **end for**
- 10: **end for**
- 11: **end for**

**Output:** relays of the inter-domain of all satellites.

where  $Ss_{a_{ij}^t}^t(D_k)$  represents the total data volume transmitted to  $a_{ij}^t(D_k)$ ,  $Rs_{a_{ij}^t}^t(D_k)$  is the data volume that can be received by  $a_{ij}^t(D_k)$ , and  $U_{a_{ij}^t}^t(D_k)$  is the number of receivers activated by  $a_{ij}^t(D_k)$ . Then the profit value minus the penalty value is defined as the reward

$$r_{ij}^t(D_k) = pr_{ij}^t(D_k) - pu_{ij}^t(D_k). \quad (40)$$

Therefore, the CDRS problem can be converted as follows:

$$\begin{aligned} \text{RCDRS: max } & \mathbb{E}_\pi \left[ \sum_{t=1}^T r_{ij}^t(D_k) \right] \\ \text{s.t. } & (33) - (36), (38) - (40). \end{aligned} \quad (41)$$

Each satellite expects to maximize the long-term reward, so as to achieve maximize the total ADTD in the satellite network.

## V. CD-DMRS ALGORITHM DESIGN

As mentioned in the previous section, the range of states is continuous and has an infinite number of possible values. We cannot get all the states and use the Bellman equation to solve. If the continuous state is discretized, the value of the state may be inaccurate. If the value of the discrete state is too much, it will cause a dimensional disaster. Therefore, the traditional

reinforcement learning method cannot be applied to our model. To deal with the aforementioned problem, DNN is adopted to approximate policy function and state-value function and we develop a CD-DMRS algorithm to solve the RCDRS problem by introducing the advantage factor and policy-oriented hyper-parameter. As shown in Fig. 5, three significant modules are introduced, i.e., the determination of relays, the acquisition of connection relationship, and DNN structure and training.

### A. Determination of Relays

In the intra-domain, each satellite selects two satellites that establish the intra-plane ISL as the relays of the intra-domain, numbered 0 and 1, and two satellites that establish the inter-plane ISL as the relays of the intra-domain numbered 2 and 3.

In the inter-domain, each satellite selects a satellite in each auxiliary domain closest to itself in the initial time slot as the relay, and numbers these satellites in turn. Algorithm 1 shows the selection steps of the relays of the inter-domain. In this paper, we number them in the order of  $D_1, D_2$ , and  $D_3$ . For example, if satellites of  $D_2$  and  $D_3$  are selected for the relays of satellites in  $D_1$ , the relay is numbered 4 in  $D_2$  and 5 in  $D_3$ . We set the earth station number after all relays. The purpose of numbering is to correspond to the output of the policy function. As shown in Fig. 5, the satellites connected by the dotted line are the relays of  $cs_{22}$  in the determining of relays of satellites module.

### B. Acquisition of Connection Relationship

Due to the orbiting movements, the network topology is time-varying, resulting in the time-varying set of available actions. We need to determine the connection relationship between satellite and earth station, and the ISCRs before selecting the policy, which can be obtained by the HSRR, so as to determine the available actions set of each satellite.

According to the intra-domain sparse representation, we first determine the relationship among  $t, t_{sta}$  and  $t_{end}$ , then use (22) or (23) to obtain the connection relationship of ISLs in intra-domain. According to the inter-domain sparse representation, we first construct the SOFM of each domain. Then, we obtain the position coordinates in the J2000.0 GICS of each satellite using (24). Finally, the connection relationship of IDLs is determined according to (29) and (30). The connection relationship of SGLs are

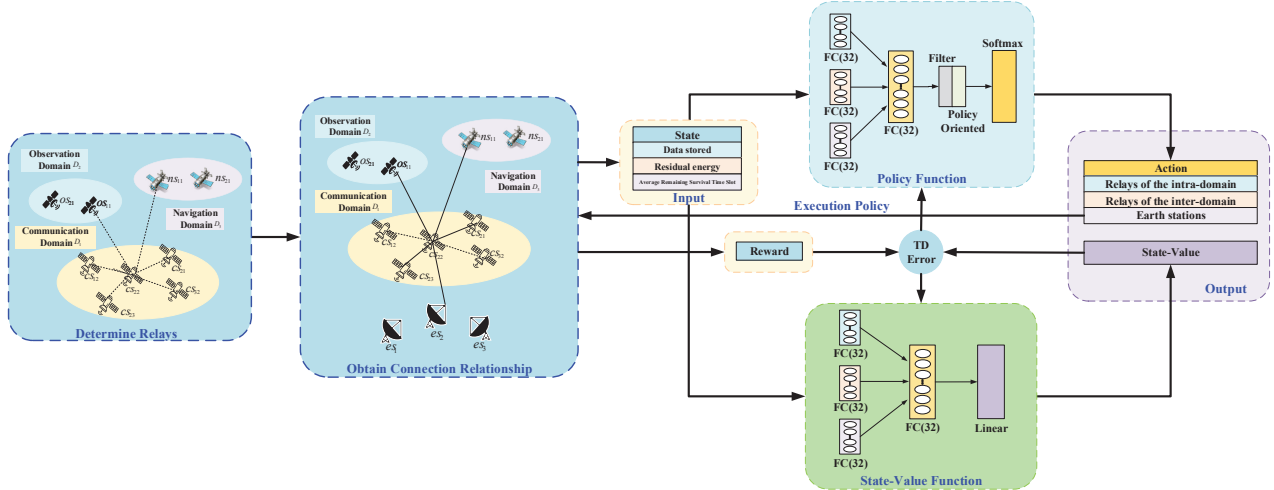


Figure 5. An overview of the CD-DMRS Algorithm.

directly obtained by STK. The set of connection relationships is  $L_{ij}^t(D_k) = [l_{ij}^t(D_k, m)]_{m \in \{\mathcal{R}_{ij}(D_k, D_{k'}) | k' = \{1, 2, 3\}\}} \cup [l_{ij}^t(D_k, es_g)]_{g \in \{1, 2, \dots, N_{es}\}}$ . As shown in Fig. 5, in the obtaining connection relationship module, the solid line indicates that a link can be established.

### C. DNN Settings And Updates

In this paper, to solve the dimensional disaster caused by continuous states, we extend the Advantage Actor-Critic (A2C) algorithm to a multi-agent network scenario and use DNN to construct policy function  $\pi_{\vartheta_{ij}}(S_{ij}^t(D_k))$  and state-value function  $V_{\varpi_{ij}}(S_{ij}^t(D_k))$ , where  $\vartheta_{ij}(D_k)$  and  $\varpi_{ij}(D_k)$  are the optimization parameters of the neural network, which include weight and bias. In the neural network input, we divide  $S_{ij}^t(D_k)$  into storage, energy, and survival time slot, which are input into separate full connection (FC) layers for processing. Then, all the outputs are combined and input into an FC layer again. The output layer is softmax for  $\pi_{\vartheta_{ij}}(S_{ij}^t(D_k))$  and linear for  $V_{\varpi_{ij}}(S_{ij}^t(D_k))$ . It should be noted that the weights and biases of  $\pi_{\vartheta_{ij}}(S_{ij}^t(D_k))$  and  $V_{\varpi_{ij}}(S_{ij}^t(D_k))$  are not shared for the same part of network structure. Moreover, to obtain available actions and form a negative gradient flow of service, we add the filter layer and policy-oriented layer before the softmax layer. As shown in Fig. 5, the DNN structure is illustrated, and the size of all layers is indicated inside parenthesis. The two functions are updated by loss functions, and the loss functions are

$$L(\varpi_{ij}(D_k)) = \frac{1}{2 \cdot |M|} \cdot \sum_{t \in M} (\widehat{r_{ij}^t}(D_k) - V_{\varpi_{ij}}(S_{ij}^t(D_k)))^2, \quad (42)$$

and

$$L(\vartheta_{ij}(D_k)) = -\frac{1}{|M|} \cdot \sum_{t \in M} \log(\pi_{\vartheta_{ij}}(a_{ij}^t(D_k) | S_{ij}^t(D_k))) \cdot W_{ij}^t(D_k), \quad (43)$$

where  $M = \{(S_{ij}^t(D_k), a_{ij}^t(D_k), r_{ij}^t(D_k), S_{ij}^{t+1}(D_k), t)\}$  is minibatch.  $|M|$  is the minibatch size.  $\widehat{r_{ij}^t}(D_k) = r_{ij}^t(D_k) + \gamma \cdot V_{\varpi_{ij}^-}(S_{ij}^{t+1}(D_k))$  is the estimated value of the state.  $\gamma \in [0, 1]$  is the discount factor.  $W_{ij}^t(D_k) = \widehat{r_{ij}^t}(D_k) - V_{\varpi_{ij}^-}(S_{ij}^t(D_k))$  is Temporal-Difference (TD) error.

For DNN training, we use the state-of-the-art orthogonal initializer [36] and use RMSprop as the gradient optimizer. Moreover, due to the importance of normalization for training DNN, we normalize the storage and energy and clip them to  $[0, 2]$ . Similarly, we normalize the reward and clip it to  $[-2, 2]$  [35].

### D. Remove Invalid Actions And Accelerate Service Offloading

1) *Remove Invalid Actions:* In the CDSR problem, due to the high dynamics of connection relationship, the available transmission links of satellites are different in each time slot, i.e., the set of available actions is different. However, since the output size of DNN is fixed, the number of action outputs from the policy function cannot be changed according to the various number of actions in the available set. Therefore, we use a filter layer to remove the invalid action. Since the output of the policy function is the probability that each action can be selected, in order to ensure that the invalid action cannot be selected, we reduce the input value of the softmax layer corresponding to the invalid action (i.e., subtract a constant from the input value, which is a hyper-parameter depending on the magnitude of the input value). Through the above method, the invalid action can be removed because the value of the negative exponent is very small, so the output probability of softmax is close to zero.

2) *Accelerate Service Offloading:* Due to the differences among service attributes, although all domains are auxiliary domains to each other, we expect that satellites with high service can offload services to auxiliary domains with low service as much as possible, and the communication resources of all domains can be fully utilized. Therefore, we add the policy-oriented layer between the filter layer and the softmax layer to form the negative gradient flow of service. Specifically, according to the data volume stored by relays, we weaken the probability of selecting a relay with a high amount of stored data and improve the probability of selecting a low amount of stored data, so as to accelerate service offload and the speed of agent learning. In this paper, we use a similar method to the

**Algorithm 2** Cross-Domain Dynamic Multi-Resource Scheduling Algorithm.

```

1: initialize  $\gamma, \eta, |M|, T, episode, \alpha_\vartheta, \alpha_\varpi, q = 0, M = \emptyset$ .
2: set  $B_{max}, E_{max}, P_{sst}, P_{set}, P_{sr}, P_o, P_h, \mathcal{RS}(D_k)$ .
3: get relays of all satellites  $\mathcal{R}_{ij}(D_k, D_{k'})$ .
4: while  $episode > 0$  do
5:   set initial states of all satellites  $S_{ij}^1(D_k)$ .
6:   for  $t = \{1, 2, \dots, T\}$  do
7:     for all satellites do
8:       get the set of connection relationships  $L_{ij}^t(D_k)$ 
       and the set of available actions  $A_{ij}^t(D_k)$ .
9:       according to the probabilities of each action to
       select a action  $a_{ij}^t(D_k)$ .
10:      end for
11:      for all satellites do
12:        use the selected action to transmit data, and get
         $pr_{ij}^t(D_k), pu_{ij}^t(D_k)$ .
13:        calculate reward  $r_{ij}^t(D_k)$ .
14:        get the next state  $S_{ij}^{t+1}(D_k)$ .
15:        store  $(S_{ij}^t(D_k), a_{ij}^t(D_k), r_{ij}^t(D_k), S_{ij}^{t+1}(D_k), t)$ 
        in  $M$ .
16:        set  $S_{ij}^t(D_k) = S_{ij}^{t+1}(D_k)$ .
17:      end for
18:       $q = q + 1$ 
19:      if  $q = |M|$  then
20:        for all satellites do
21:          calculate estimated state-value  $\widehat{r_{ij}^t}(D_k)$ .
22:          use loss functions to update  $\varpi_{ij}(D_k)$  and
           $\vartheta_{ij}(D_k)$ .
23:        end for
24:         $q = 0, M = \emptyset$ .
25:      end if
26:    end for
27:     $episode = episode - 1$ .
28:  end while

```

filter layer (i.e., introduce the policy-oriented hyper-parameter) to increase the input value of the softmax layer corresponding to the action that we want to select according to the set of available actions, so as to realize the policy orientation.

To sum up, the proposed CD-DMRS algorithm is shown in Algorithm 2. In the algorithm, an episode includes  $T$  time slots.  $\alpha_\vartheta$  and  $\alpha_\varpi$  are the learning rates for  $\pi_{\vartheta_{ij}}(S_{ij}^t(D_k))$  and  $V_{\varpi_{ij}}(S_{ij}^t(D_k))$ . Each satellite first obtains the relays  $\mathcal{R}_{ij}(D_k, D_{k'})$  according to Section V-A. Moreover, we reinitialize the state information of all satellites for each episode.  $L_{ij}^t(D_k)$  is obtained according to Section V-B, and whether the link can be established is expressed in binary, 1 if established and 0 otherwise. In addition, we assume that all satellites can make decisions and transmit data at the same time. In the process of resource scheduling, due to the difference of service attributes among domains, to ensure the effective scheduling of resources, the proposed algorithm can dynamically adjust the transmission policy of satellites of each domain according to the state of relays.

## VI. SIMULATION RESULTS AND DISCUSSIONS

In this section, extensive simulations are carried out to evaluate the proposed CD-DMRS algorithm. Specifically, it includes two parts: (1) Analyze the scheduling performance of the CD-DMRS algorithm under different parameters. (2) Compare the RUR and RUE under different algorithms. To compare the performance, four additional approaches are considered:

- Non-CD-DMRS (NCD-DMRS): The algorithm is implemented in the framework of the CD-DMRS algorithm. The difference is that the set of available actions does not include relays of satellites in the auxiliary domains.
- Independent A2C (IA2C) [37]: In this scheme, satellites do not share state information with each other, and only complete the policy selection through their own state. In other words, each satellite's observation of the environment is inconsistent.
- Extended Deep Q-Network (EDQN) [38]: In this scheme, we adopt the theory of the DQN algorithm and extend it to our model to realize the application of DQN in the multi-agent network scenario.
- Fair Transmission Selection (FTS): In this scheme, all available actions can be selected fairly, which means that each satellite has a fair opportunity to select relays and earth stations.

### A. Simulation Configuration

We conduct experiments on a satellite network scenario with three domains. Specifically, according to the orbit parameters of Iridium communication system, OSTM/Jason-2 observation satellite and GLONASS navigation system, we set that 66 communication satellites are evenly distributed over six low earth orbits at a height of 780Km and with inclination 86.4° in  $D_1$ , 48 observation satellites are evenly distributed over eight low earth orbits at a height of 1336Km and with inclination 66° in  $D_2$ , and 24 navigation satellites are evenly distributed over three medium earth orbits at a height of 19100Km and with inclination 64.8° in  $D_3$ . Five earth stations are located at Kashi (39.5°N, 76°E), Xi'an (34°N, 108°E), Sanya (18°N, 109.5°E), Beijing (40°N, 116°E) and Qingdao (36°N, 120°E), and we assume that data sharing can be realized among the earth stations. The duration of planning cycle is 6 hours. Furthermore, we utilize STK to obtain all connection relationships of SGLs from 19 Nov. 2021 04:00:00 to 19 Nov. 2021 10:00:00 which can be used to determine the set of available actions in the planning cycle. In the simulations, we set  $\tau = 100s$ ,  $T = 216$ ,  $P_{sst} = 20W$ ,  $P_{set} = 20W$ ,  $P_{sr} = 10W$ ,  $P_o = 5W$ ,  $P_h = 20W$ ,  $\eta = 75\%$ . Moreover, according to [30] and [31], the ISL/IDL transmission rate is distributed within [80, 160]Mbps and the SGL transmission rate is 60Mbps. Besides, we set the SGL transmission bandwidth  $\mathcal{B} = 250\text{MHz}$ ,  $B_{max} = 60\text{Gbits}$ ,  $E_{max} = 60\text{KJ}$ ,  $\mathcal{RS}(D_1) = 18$ ,  $\mathcal{RS}(D_2) = 72$ , and  $\mathcal{RS}(D_3) = 6$ . We set that the data arrival for communication satellites is  $\lambda_{ij}(D_1) = 0.7$  and  $\rho_{ij}(D_1) = 5\text{Gbits}$ , for observation satellites is  $\rho_{ij}(D_2) = 6\text{Gbits}$  and for navigation satellites is  $\rho_{ij}(D_3) = 0.5\text{Gbits}$ . Moreover, for DNN training, we set  $episode = 500$ ,  $\gamma = 0.99$ ,  $\alpha_\varpi = 1e-4$ ,  $\alpha_\vartheta = 3e-4$  and

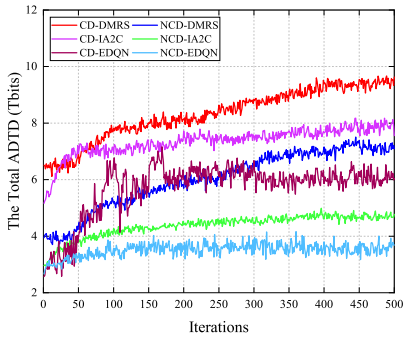


Figure 6. Convergence performance of the CD-DMRS, NCD-DMRS and existing algorithms.

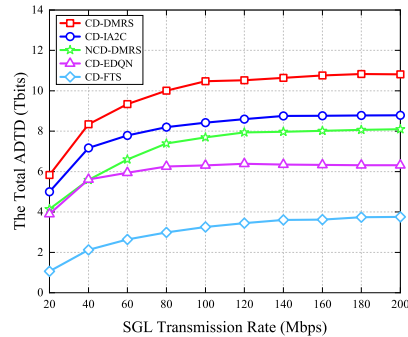


Figure 7. The total ADTD versus SGL transmission rate with  $B_{max} = 60$ Gbits and  $E_{max} = 60$ KJ.

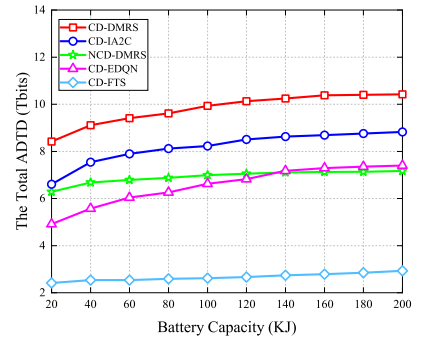


Figure 8. The total ADTD versus  $E_{max}$  with  $B_{max} = 60$ Gbits.

$|M| = 72$ , and the advantage factors of the three domains are  $\delta_{ij}(D_1) = 1$ ,  $\delta_{ij}(D_2) = 10$  and  $\delta_{ij}(D_3) = 100$ , respectively. Furthermore, we set  $\zeta_{ij}(D_1, m) = 0.2$ ,  $m \in \mathcal{R}_{ij}(D_1, D_2)$ ,  $\zeta_{ij}(D_1, m) = 0.6$ ,  $m \in \mathcal{R}_{ij}(D_1, D_3)$ ,  $\zeta_{ij}(D_2, m) = -0.01$ ,  $m \in \mathcal{R}_{ij}(D_2, D_1)$ ,  $\zeta_{ij}(D_2, m) = 0.03$ ,  $m \in \mathcal{R}_{ij}(D_2, D_3)$ ,  $\zeta_{ij}(D_3, m) = -0.001$ ,  $m \in \mathcal{R}_{ij}(D_3, D_1)$ , and  $\zeta_{ij}(D_3, m) = -0.002$ ,  $m \in \mathcal{R}_{ij}(D_3, D_2)$ . For NCD-DMRS algorithm,  $\alpha_{\varpi} = 2e - 4$ ,  $\alpha_{\vartheta} = 5e - 4$ .

### B. Performance Evaluation

Figure 6 shows the convergence performance of algorithms under cross-domain and non-cross-domain scenarios<sup>9</sup>. It can be seen that the total ADTD obtained by the proposed algorithm during training fluctuates rise with the optimization of the CDRS policy and finally converges and stabilizes with the small fluctuations. Furthermore, at the beginning of the iteration, the network has a low total ADTD and poor system performance for all algorithms. With the number of iterations increasing, satellites learn better policy makes the total ADTD of the whole network gradually increase. Moreover, the CD-DMRS algorithm has the best learning ability.

Figure 7 shows the total ADTD for different SGL transmission rates. It can be seen that with the rate increase, the performance of the CD-DMRS algorithm is better than the existing algorithms, and the total ADTD increases gradually. Moreover, since the transmission rate is directly proportional to the transmission power, for a large rate, the battery capacity of the satellite is limited, and the excessive use of energy leads to the total ADTD cannot continue to increase. In this case, CD-EDQN and CD-FTS algorithms cannot reasonably select the data transmission policy, resulting in insufficient energy to be used when data needs to be downloaded. Besides, since the CD-IA2C algorithm only makes decisions based on its state information, its performance is worse than that of the CD-DMRS algorithm.

We also investigate the impact of battery capacity on system performance as shown in Fig. 8. Similarly, the CD-DMRS algorithm has better performance and with the increase of battery capacity, the total ADTD of all algorithms increases

<sup>9</sup>Since the total ADTD of non-cross-domain is less than cross-domain, we only take the results of the NCD-DMRS algorithm as an example in this subsection.

Table II  
THE ADTD UNDER DIFFERENT DELAY DEMAND CONFIGURATIONS.

Delay demand ( $\mathcal{RS}(D_k)$ )	ADTD (Tbits)			
	$D_1/D_2/D_3$	Communication data	Observation data	Navigation data
6/24/2		4.677	1.043	1.518
12/48/4		5.413	1.137	1.603
18/72/6		6.133	1.157	1.709
24/96/8		6.279	1.020	1.731
30/120/10		6.412	1.104	1.730
36/144/12		6.626	1.009	1.698

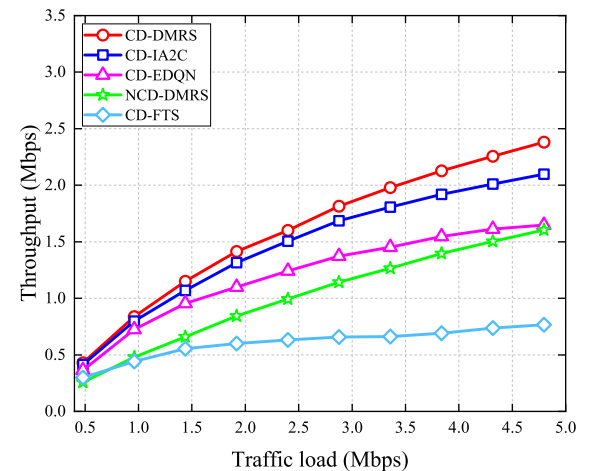


Figure 9. The throughput under different single-satellite traffic loads.

gradually. The reason lies in that satellites have a greater battery capacity to harvest more energy to ensure sufficient available energy when transmitting data to the earth station. In addition, the scheduling policy selected by the CD-EDQN algorithm may waste too much energy for inter-satellite transmission, so it has worse performance than the NCD-CDMS algorithm when the battery capacity is low. The CD-FTS algorithm cannot select the transmission policy according to the satellite resource states, so the increase of battery capacity cannot bring significant gain.

Table II shows the ADTD under different delay demand configurations. It can be seen that with the increasing  $\mathcal{RS}(D_k)$ , the ADTD of communication data gradually

Table III  
CDRS PERFORMANCE UNDER DIFFERENT SERVICE DEMAND CONFIGURATIONS.

Sequence	Proportion	Service demand configuration mode	Total ADTD (Tbits)		Gain (Tbits)
			CD-DMRS	NCD-DMRS	
1	1 : 1 : 1	$\lambda_{ij}(D_1) = 0.2, \rho_{ij}(D_1) = 0.5, \rho_{ij}(D_2) = 1.5, \rho_{ij}(D_3) = 0.25$	3.121	2.978	0.143
2	2 : 1 : 1	$\lambda_{ij}(D_1) = 0.4, \rho_{ij}(D_1) = 0.5, \rho_{ij}(D_2) = 1.5, \rho_{ij}(D_3) = 0.25$	4.093	3.344	0.749
3	4 : 1 : 1	$\lambda_{ij}(D_1) = 0.4, \rho_{ij}(D_1) = 1, \rho_{ij}(D_2) = 1.5, \rho_{ij}(D_3) = 0.25$	5.495	4.112	1.383
4	4 : 2 : 1	$\lambda_{ij}(D_1) = 0.4, \rho_{ij}(D_1) = 1, \rho_{ij}(D_2) = 3, \rho_{ij}(D_3) = 0.25$	5.641	4.725	0.916
5	6 : 1 : 1	$\lambda_{ij}(D_1) = 0.6, \rho_{ij}(D_1) = 1, \rho_{ij}(D_2) = 1.5, \rho_{ij}(D_3) = 0.25$	6.379	3.912	2.467
6	6 : 2 : 1	$\lambda_{ij}(D_1) = 0.6, \rho_{ij}(D_1) = 1, \rho_{ij}(D_2) = 3, \rho_{ij}(D_3) = 0.25$	6.605	4.860	1.745

Table IV  
CDRS PERFORMANCE UNDER DIFFERENT COMMUNICATION RESOURCE CONFIGURATIONS.

Sequence	Proportion	Communication resource configuration mode	Total ADTD (Tbits)		Gain (Tbits)
			CD-DMRS	NCD-DMRS	
1	1 : 1 : 1	$D_1 : 90, D_2 : 60, D_3 : 30$	9.620	7.782	1.838
2	2 : 4 : 3	$D_1 : 60, D_2 : 80, D_3 : 30$	9.037	6.769	2.268
3	2 : 3 : 4	$D_1 : 60, D_2 : 60, D_3 : 40$	9.337	6.712	2.625
4	1 : 5 : 3	$D_1 : 30, D_2 : 100, D_3 : 30$	7.971	5.221	2.750
5	1 : 3 : 5	$D_1 : 30, D_2 : 60, D_3 : 50$	8.382	5.272	3.110
6	1 : 4 : 4	$D_1 : 30, D_2 : 80, D_3 : 40$	8.379	5.365	3.014

increases, and the growth rate is fast at first and then slow. The observation data and navigation data both increased first and then decreased, which may be because  $D_1$  seeks the  $D_2$  and  $D_3$  to assist data offloading and the  $\mathcal{R}S(D_k)$  of communication data gradually increases so that the storage space of observation satellites and navigation satellites has the high occupation to reduce the amount of observation data and navigation data stored.

Figure 9 shows the throughput under different single-satellite traffic loads. It can be seen that the CD-DMRS algorithm obtains the highest throughput under the premise of satisfying the delay demands. Furthermore, with the increasing traffic load, the throughput reached by all algorithms is gradually increasing and the growth rate is gradually slowing down, and the gap between throughput and traffic load is becoming larger and larger. Besides, the CD-EDQN algorithm may carry out frequent inter-satellite transmission so that the performance of the CD-EDQN algorithm drops significantly with the increasing traffic load.

Table III shows CDRS performance under different service demand configurations. It can be seen that CD-DMRS and NCD-DMRS algorithms have similar performance in mode 1, when the resources of each domain can meet the service demands, and there is no difference in the service demands among domains. Moreover, with the enhancement of the service demand difference, the CD-DMRS algorithm shows better performance and improves the network resources utilization through resource cooperation among domains, the greater the service demand difference, the more significant the performance improvement of CD-DMRS compared with NCD-DMRS. In addition, mode 4 (6) obtains more total ADTD than mode 3 (5) but does not obtain a higher gain. The reason lies in that the  $D_2$  produces higher service demands, which limits the  $D_2$  to assist the  $D_1$  in data transmission.

CDRS performance under different communication resource configurations is shown in Table IV. It can be seen that since the  $D_2$  and  $D_3$  assist data transmission of the  $D_1$ , the CD-

DMRS algorithm achieves significant gain in mode 1, when there is no difference in resources among domains. Moreover, with the enhancement of resource difference, the CD-DMRS algorithm shows better performance, the greater the resource difference, the more significant the performance improvement of CD-DMRS compared with NCD-DMRS. In addition, due to the influence of the visible time slots caused by the orbit altitudes, the data volume that can be offloaded from the  $D_1$  to the  $D_2$  is less than that of the  $D_3$ , resulting in significant differences in the total ADTD of the CD-DMRS algorithm under the condition of the same resource promotion.

### C. Resource Utilization Evaluation

To verify the effectiveness of the proposed algorithm in resource utilization, we compared the total ADTD, RUR, and RUE of different algorithms as shown in Fig. 10. It can be observed from Fig. 10(a) and Fig. 10(b) that the CD-DMRS algorithm achieves the highest total ADTD and RUR under both demands, and due to the lower demand, the RUR of all algorithms decreases for  $\rho_{ij}(D_1) = 2.5$ . Furthermore, the RUR of the CD-IA2C algorithm is not much different from that of the CD-DMRS algorithm, but the total ADTD is much lower. The reason lies in that the CD-IA2C algorithm has poor RUE, and resources are used ineffectively.

As mentioned above, the level of RUR does not fully represent the effectiveness of resources. Therefore, the CRUE and ERUE under different algorithms are shown in Fig. 10(c). It can be seen that the utilization efficiency of the CD-DMRS algorithm is much higher than other algorithms whether it is the communication resource or energy resource, and the CD-IA2C algorithm with higher RUE achieves better performance than the CD-EDQN and CD-FTS algorithms. Moreover, it is foreseeable that the CRUE of all algorithms is reduced due to the lower demand.

To sum up, the proposed CD-DMRS algorithm can achieve reasonable allocation and efficient utilization of resources for the whole network by coordinating the CDRS policy.

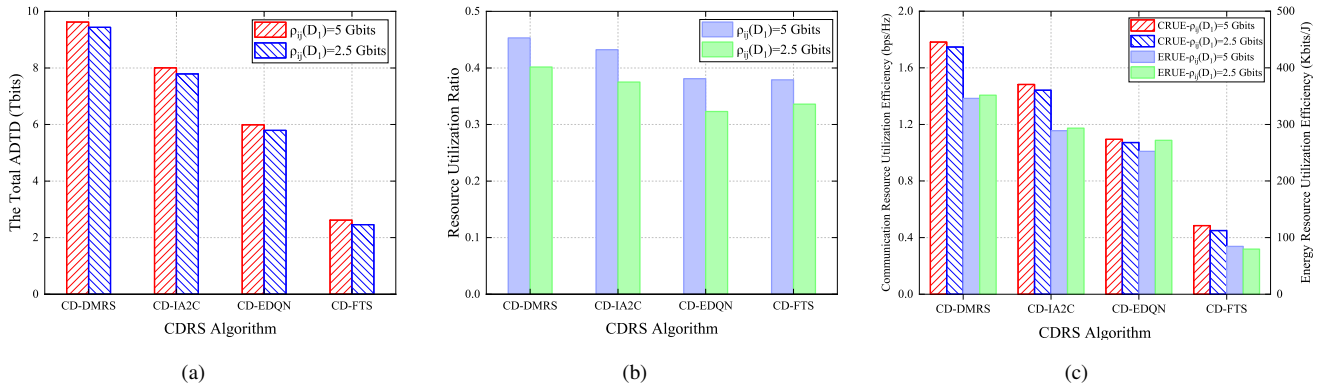


Figure 10. Resource Utilization Evaluation. (a) The total ADTD under different CDRS algorithms. (b) Resource utilization ratio under different CDRS algorithms. (c) Communication resource utilization efficiency (CRUE) and energy resource utilization efficiency (ERUE) under different CDRS algorithms.

## VII. CONCLUSION

In this paper, we have investigated the CDRS problem for satellite networks. Starting from the orbit motion characteristics of satellites and utilizing the periodicity and rotational closure of the ISCR, we design the HSRR scheme to accurately characterize the resource state of the network in real-time with much lower space complexity than existing representation schemes. Further, thanks to the real-time characteristics of HSRR, we develop a CD-DMRS algorithm to solve the CDRS problem by introducing the advantage factor and policy-oriented hyper-parameter. The algorithm can dynamically adjust the scheduling policy to achieve efficient CDRS. Simulation results show that the greater the service demand and resource difference among domains, the more significant the performance improvement brought by CDRS to the satellite network, and the proposed CD-DMRS algorithm proves the necessity of CDRS to improve the RUR of the satellite network.

## REFERENCES

- [1] L. Liu, E. G. Larsson, W. Yu, P. Popovski, C. Stefanovic, and E. de Carvalho, "Sparse signal processing for grant-free massive connectivity: A future paradigm for random access protocols in the internet of things," *IEEE Signal Process Mag.*, vol. 35, no. 5, pp. 88–99, Sept. 2018.
- [2] W. Saad, M. Bennis, and M. Chen, "A vision of 6G wireless systems: Applications, trends, technologies, and open research problems," *IEEE Network*, vol. 34, no. 3, pp. 134–142, May/June 2020.
- [3] Q. Wu, W. Chen, D. W. K. Ng, and R. Schober, "Spectral and energy-efficient wireless powered IoT networks: NOMA or TDMA?" *IEEE Trans. Veh. Technol.*, vol. 67, no. 7, pp. 6663–6667, July 2018.
- [4] X. Li, W. Feng, J. Wang, Y. Chen, N. Ge, and C.-X. Wang, "Enabling 5G on the ocean: A hybrid satellite-UAV-terrestrial network solution," *IEEE Wireless Commun.*, vol. 27, no. 6, pp. 116–121, Dec. 2020.
- [5] J. Liu, Y. Shi, Z. M. Fadlullah, and N. Kato, "Space-air-ground integrated network: A survey," *IEEE Commun. Surv. Tutorials*, vol. 20, no. 4, pp. 2714–2741, May 2018.
- [6] Z. Zhang, Y. Xiao, Z. Ma, M. Xiao, Z. Ding, X. Lei, G. K. Karagiannidis, and P. Fan, "6G wireless networks: Vision, requirements, architecture, and key technologies," *IEEE Veh. Technol. Mag.*, vol. 14, no. 3, pp. 28–41, July 2019.
- [7] D. Zhou, M. Sheng, Y. Wang, J. Li, and Z. Han, "Machine learning-based resource allocation in satellite networks supporting internet of remote things," *IEEE Transactions on Wireless Communications*, vol. 20, no. 10, pp. 6606–6621, Oct. 2021.
- [8] N.-N. Dao, Q.-V. Pham, N. H. Tu, T. T. Thanh, V. N. Q. Bao, D. S. Lakew, and S. Cho, "Survey on aerial radio access networks: Toward a comprehensive 6G access infrastructure," *IEEE Commun. Surv. Tutorials*, vol. 23, no. 2, pp. 1193–1225, Feb. 2021.
- [9] J. Radtke, C. Kebschull, and E. Stoll, "Interactions of the space debris environment with mega constellations - using the example of the OneWeb constellation," *Acta Astronaut.*, vol. 131, pp. 55–68, Feb. 2017.
- [10] T. Pultarova, "Telecommunications - space tycoons go head to head over mega satellite network [news briefing]," *Eng. Technol.*, vol. 10, no. 2, p. 20, Mar. 2015.
- [11] Y. Su, Y. Liu, Y. Zhou, J. Yuan, H. Cao, and J. Shi, "Broadband LEO satellite communications: Architectures and key technologies," *IEEE Wireless Commun.*, vol. 26, no. 2, pp. 55–61, Apr. 2019.
- [12] D. Zhou, M. Sheng, J. Wu, J. Li, and Z. Han, "Gateway placement in integrated satellite-terrestrial networks: Supporting communications and internet of remote things," *IEEE Internet Things J.*, Accepted, 2021.
- [13] J. Qi, J. Guo, M. Wang, and C. Wu, "A cooperative autonomous scheduling approach for multiple earth observation satellites with intensive missions," *IEEE Access*, vol. 9, pp. 61 646–61 661, Apr. 2021.
- [14] L. Zhu, D. Guo, J. Yin, G. V. Steeg, and A. Galstyan, "Scalable temporal latent space inference for link prediction in dynamic social networks," *IEEE Trans. Knowl. Data Eng.*, vol. 28, no. 10, pp. 2765–2777, July 2016.
- [15] T. Zhu, P. Li, L. Yu, K. Chen, and Y. Chen, "Change point detection in dynamic networks based on community identification," *IEEE Trans. Network Sci. Eng.*, vol. 7, no. 3, pp. 2067–2077, Feb. 2020.
- [16] E. Cakmak, U. Schlegel, D. Jäckle, D. Keim, and T. Schreck, "Multiscale snapshots: Visual analysis of temporal summaries in dynamic graphs," *IEEE Trans. Visual Comput. Graphics*, vol. 27, no. 2, pp. 517–527, Feb. 2021.
- [17] Y.-Q. Zhang, X. Li, J. Xu, and A. V. Vasilakos, "Human interactive patterns in temporal networks," *IEEE Trans. Syst. Man Cybern.: Syst.*, vol. 45, no. 2, pp. 214–222, Feb. 2015.
- [18] Z. Tang, Z. Feng, W. Han, W. Yu, B. Zhao, and C. Wu, "Improving the snapshot routing performance through reassigning the inter-satellite links," in *Proc. INFOCOM WKSHPS*, Hong Kong, China, Apr. 2015, pp. 97–98.
- [19] F. Jiang, Q. Zhang, Z. Yang, and P. Yuan, "A space-time graph based multipath routing in disruption-tolerant earth-observing satellite networks," *IEEE Trans. Aerosp. Electron. Syst.*, vol. 55, no. 5, pp. 2592–2603, Oct. 2019.
- [20] P. Yuan, Z. Yang, Y. Li, and Q. Zhang, "An event-driven graph-based min-cost delivery algorithm in earth observation DTN networks," in *Proc. WCSP*, Nanjing, China, Oct. 2015, pp. 1–6.
- [21] T. Zhang, J. Li, H. Li, S. Zhang, P. Wang, and H. Shen, "Application of time-varying graph theory over the space information networks," *IEEE Network*, vol. 34, no. 2, pp. 179–185, Feb. 2020.
- [22] S. Haiquan, X. Wei, H. Xiaoxuan, and X. Chongyan, "Earth observation satellite scheduling for emergency tasks," *J. Syst. Eng. Electron.*, vol. 30, no. 5, pp. 931–945, Oct. 2019.
- [23] D. Zhou, M. Sheng, B. Li, J. Li, and Z. Han, "Distributionally robust planning for data delivery in distributed satellite cluster network," *IEEE Trans. Wireless Commun.*, vol. 18, no. 7, pp. 3642–3657, July 2019.
- [24] X. Wang, C. Han, R. Zhang, and Y. Gu, "Scheduling multiple agile earth observation satellites for oversubscribed targets using complex networks theory," *IEEE Access*, vol. 7, pp. 110 605–110 615, June 2019.
- [25] L. He, J. Li, M. Sheng, R. Liu, K. Guo, and D. Zhou, "Dynamic scheduling of hybrid tasks with time windows in data relay satellite

- networks," *IEEE Trans. Veh. Technol.*, vol. 68, no. 5, pp. 4989–5004, May 2019.
- [26] X. Chen, X. Li, X. Wang, Q. Luo, and G. Wu, "Task scheduling method for data relay satellite network considering breakpoint transmission," *IEEE Trans. Veh. Technol.*, vol. 70, no. 1, pp. 844–857, 2021.
- [27] R. Liu, M. Sheng, K. Lui, X. Wang, D. Zhou, and Y. Wang, "Capacity of two-layered satellite networks," *Wireless Networks*, vol. 23, pp. 2651–2669, Nov. 2017.
- [28] Q. Chen, G. Giambene, L. Yang, C. Fan, and X. Chen, "Analysis of inter-satellite link paths for LEO mega-constellation networks," *IEEE Trans. Veh. Technol.*, vol. 70, no. 3, pp. 2743–2755, Mar. 2021.
- [29] J. L. Laso Fernández, "Study, modelling and design of intersatellite links (ISL) in millimeter-wave band/estudio, modelado y diseño de enlaces intersatelitales (ISL) en bandas de milimétricas," *Telecomunicacion*, July 2020.
- [30] A. Golkar and I. Lluch i Cruz, "The federated satellite systems paradigm: Concept and business case evaluation," *Acta Astronautica*, vol. 111, pp. 230–248, June 2015.
- [31] D. Zhou, M. Sheng, R. Liu, Y. Wang, and J. Li, "Channel-aware mission scheduling in broadband data relay satellite networks," *IEEE J. Sel. Areas Commun.*, vol. 36, no. 5, pp. 1052–1064, May 2018.
- [32] J. Navarro-Ortiz, P. Romero-Díaz, S. Sendra, P. Ameigeiras, J. J. Ramos-Munoz, and J. M. Lopez-Soler, "A survey on 5G usage scenarios and traffic models," *IEEE Commun. Surv. Tutorials*, vol. 22, no. 2, pp. 905–929, Second quarter 2020.
- [33] V. Kartashevskiy and M. Buranova, "Analysis of packet jitter in multi-service network," in *Proc. PIC S&T*, Kharkiv, Ukraine, Oct. 2018, pp. 797–802.
- [34] C. Bao, D. Zhou, M. Sheng, Y. Shi, and J. Li, "Resource scheduling in satellite networks: A sparse representation based machine learning approach," in *Proc. IEEE GLOBECOM*, Madrid, Spain, Dec. 2021.
- [35] T. Chu, J. Wang, L. Codecà, and Z. Li, "Multi-agent deep reinforcement learning for large-scale traffic signal control," *IEEE Trans. Intell. Transp. Syst.*, vol. 21, no. 3, pp. 1086–1095, Mar. 2020.
- [36] A. M. Saxe, J. L. McClelland, and S. Ganguli, "Exact solutions to the nonlinear dynamics of learning in deep linear neural networks," *arXiv preprint arXiv:1312.6120*, Dec. 2013.
- [37] V. Mnih, A. P. Badia, M. Mirza, A. Graves, T. Lillicrap, T. Harley, D. Silver, and K. Kavukcuoglu, "Asynchronous methods for deep reinforcement learning," in *Int. Conf. Mach. Learn.*, June 2016, pp. 1928–1937.
- [38] J. Z. Leibo, V. Zambaldi, M. Lanctot, J. Marecki, and T. Graepel, "Multi-agent reinforcement learning in sequential social dilemmas," *arXiv preprint arXiv:1702.03037*, Feb. 2017.



**Di Zhou** (M'19) received the B.E. and the Ph.D. degrees in communication and information systems from Xidian University, Xi'an, China, in 2013 and 2019, respectively. She was also a Visiting Ph.D. Student with the Department of Electrical and Computer Engineering, University of Houston, from 2017 to 2018. She is currently an Associate Professor with the State Key Laboratory of Integrated Service Networks, Xidian University. Her research interests include dynamic resource allocation, mission planning, and performance evaluation in space-terrestrial integration networks and space information networks.



**Yan Shi** (M'10) received the Ph.D. degree from Xidian University, Xi'an, China, in 2005. He is currently a Full Professor with the State Key Laboratory of Integrated Service Networks, Xidian University. His current research interests include cognitive networks, modern switching technologies, and distributed wireless networking.



**Chenxi Bao** received the B.E. degree in communication engineering from Tiangong University, Tianjin, China, in 2020. She is currently working toward the Ph.D. degree in information and communications engineering. Her research interests include resource representation and dynamic resource scheduling in satellite networks.



**Min Sheng** (M'03, SM'16) joined Xidian University in 2000, where she is currently a Full Professor and Director of the State Key Laboratory of Integrated Services Networks. She is the Vice Chair of IEEE Xi'an Section. She is an Editor for IEEE Communications Letters and IEEE Trans. on Wireless Communications. She has published over 200 refereed papers in international leading journals and key conferences in the area of wireless communications and networking. Her current research interests include Space-Terrestrial Integration networks, intelligent wireless networks, and mobile ad hoc networks. She received China National Funds for Distinguished Young Scientists in 2018.



**Jiandong Li** (M'96-SM'05-F'20) received the B.E., M.S. and Ph.D. degrees in Communications Engineering from Xidian University, Xi'an, China, in 1982, 1985 and 1991 respectively. He has been a faculty member of the school of Telecommunications Engineering at Xidian University since 1985, where he is currently a professor and vice director of the academic committee of State Key Laboratory of Integrated Service Networks. He was a visiting professor to the Department of Electrical and Computer Engineering at Cornell University from 2002-2003.

He served as the General Vice Chair for ChinaCom 2009 and TPC Chair of IEEE ICCC 2013. He was awarded as Distinguished Young Researcher from NSFC and Changjiang Scholar from Ministry of Education, China, respectively. His major research interests include wireless communication theory, cognitive radio and signal processing.